



The continuation and stability analysis methods for quasi-periodic solutions of nonlinear systems

Haitao Liao · Quanyue Zhao · Daining Fang

Received: 18 November 2019 / Accepted: 15 January 2020 / Published online: 8 April 2020
© Springer Nature B.V. 2020

Abstract The continuation and stability analysis methods for quasi-periodic solutions of nonlinear systems are proposed. The proposed continuation method advances the predictor–corrector continuation framework by coupling the reduced space sequential quadratic programming method with the multi-dimensional harmonic balance method and the gradients required for the continuation problem are derived. In order to determine the stability of quasi-periodic solution, a novel approach based on the analytical formulation of the harmonic balance equations is presented by using the Floquet theory with the perturbation term applied to the known quasi-periodic solution. Sensitivity analysis about the stability factor of quasi-periodic solution is also carried out. Finally, the effectiveness and applicability of the proposed methodology is verified and illustrated by two numerical examples. The proposed approaches have been demonstrated to be able to trace

the aperiodic solutions of nonlinear systems and analyze their stabilities.

Keywords Quasi-periodic solution · Reduced space SQP method · Multi-dimensional harmonic balance method · Continuation · Stability

1 Introduction

The search for periodic or quasi-periodic solutions in nonlinear dynamical systems has a long standing tradition [1–5]. The harmonic balance method has been successfully applied to analyze the nonlinear structural vibrations and related problems [6–10]. For example, the incremental harmonic balance method is recently revisited in Ref. [11] to investigate the dynamic properties and stabilities of two-degree-of-freedom (DOF) vehicle system with quadratic and cubic stiffness nonlinearities. Recently, Liao [12, 13] presented the harmonic balance-based constraint optimization framework for searching the worst-case resonance response where the vibration frequency is considered as optimization variable. The reduced space approach to circumvent the drawbacks such as the computational efficiency of the previous works is investigated in Ref. [14]. The key idea of the reduced space method is to decompose nonlinear equality constraints to null and range spaces, leading to the bound constraint optimization problem needed to be solved.

It is often of interest to determine how the solutions of structural systems evolve under variation of struc-

H. Liao (✉) · Q. Zhao
Institute of Advanced Structure Technology, Beijing
Institute of Technology, Beijing 100081, China
e-mail: ht0819@163.com

Q. Zhao
Beijing Key Laboratory of Lightweight Multi-functional
Composite Materials and Structures, Beijing Institute of
Technology, Beijing 100081, China

D. Fang
State Key Laboratory of Explosion Science and
Technology, Beijing Institute of Technology,
Beijing 100081, China

tural free parameter. The evolution of the solutions can be tracked by using the numerical continuation method [15, 16], which is usually adopted for solving the system of nonlinear algebraic equations with parameter variation. The continuation method is achieved by augmenting the system of algebraic equations with suitable constraint condition(s) and free parameter(s). The task of numerical path continuation methods is to generate a sequence of suitably solution points with respect to the free parameter. The standard procedure of the predictor–corrector continuation scheme consists of two steps. For the predictor step, a prediction from the current solution point is generated in the direction of the tangent to the solution branch by using the predictor procedure and the prediction solution is corrected at the corrector step by using the root-finding algorithm to obtain a next point on the solution branch. Repeated application of the predictor–corrector step traces out the entire solution set over the parameter space. Various predictive approaches and path parametrization strategies have been developed and the interested reader is referred to Ref. [17] for more details about the continuation technique.

Many nonlinear vibration problems are investigated by utilizing the continuation method. For example, the nonlinear dynamics of Dielectric elastomers have been studied in Ref. [18] by combining the shooting method with the pseudo-arc length continuation. Nevertheless, there are several underlying challenges associated with the shooting-based continuation method in general: the complexity and simulation time appears to scale with the dimension of nonlinear system. These shortcomings make frequency-domain harmonic balance method appealing. For instance, the continuation of antiresonance response is investigated in Ref. [19] via the harmonic balance method with a continuation technique. The higher-order harmonic balance method for the continuation of periodic motions is developed in Ref. [20]. Guillot et.al [21] proposed a generic Taylor series-based continuation method to compute the bifurcation diagrams of nonlinear systems. In Ref. [22], the harmonic balance method is combined with the asymptotic numerical method (ANM) to follow the periodic solutions of delay differential equations. Within the framework of asymptotic numerical method, the auxiliary variables and additional equations are needed to express the differential/algebraic equation system in quadratic form. However, the artificial/spurious solution may be introduced due to the quadratic recast

Furthermore, increasing the dimension of the differential/algebraic equations can result in a very large number of differential/algebraic equations to be solved, leading to numerically challenge for the computational cost (even the convergence problem is encountered).

Up to now, analysis of quasi-periodic motions in nonlinear systems gains more and more attention in nonlinear dynamics community [23]. Awrejcewicz and Reinhardt [24, 25] have conducted some earliest and important researches on nonlinear dynamics of aperiodic solutions. With the use of the double perturbation method for theoretical analysis and the generalized Poincaré map for numerical calculation, both the analytical and numerical approaches to search quasi-periodic solutions of nonlinear systems are presented in Ref. [26]. Recently, an integral equation approach [27] which combines the Picard iteration and the Newton–Raphson scheme to solve the integral equations has been developed to approximate periodic or quasi-periodic responses of nonlinear systems and intensive numerical integration calculation can be alleviated. Huang et al. [28] studied the quasi-periodic solutions of the fixed-fixed translating beam equations via the incremental harmonic balance methodology and the Floquet theory along with the precise Hsu’s method is used to investigate the stability of periodic responses. The incremental harmonic balance method is modified and implemented in Ref. [29] to analyze quasi-periodic aeroelastic motions of an airfoil with an external store. A solving strategy by applying the harmonic balance method to search the quasi-periodic solutions of nonlinear systems is reported in Ref. [30]. Kim and Noah [31] studied the quasi-periodic response of a non-smooth Jeffcott rotor system with bearing clearance and quasi-periodic response is confirmed to appear in the Jeffcott rotor system. The harmonic balance methodology is extended in Ref. [32] to study the localization quasi-periodic motions of cyclic structures. In order to locate the isolated solutions in the global parameter space, a hybrid method which incorporates the advantages of global exploration and local exploitation is developed in Ref. [33]. The harmonic balance technique has been successfully applied for the numerical continuation of quasi-periodic solution in Ref. [34] and works are focused on the quasi-periodic response characteristics of the piecewise smooth rotor/stator rubbing systems. In Ref. [35], a harmonic balance approach is presented for detecting and tracing quasi-periodic solutions with two frequencies and an assumption is made

on the initial condition such that the initial velocities are taken to be zero.

It should be noted that the predictor–corrector solver in all previous mentioned continuation methods are resorted to the root-finding approach. However, there are open questions about the application of the Newton-type predictor–corrector solver, and many challenging aspects are still pending owing to the complex dynamical behaviors of nonlinear systems. During the continuation process, the continuation parameters are set as optimization variables. The prediction technique is usually applied in order to obtain a reliable initial guess via the root-finding method which is employed to correct the prediction solution. In order to apply the root-finding algorithm for correction, it is required that the number of nonlinear equations is the same as that of the unknowns. However, the number of unknown variables is greater than or equal to the number of original equations, which are under-determined. Therefore, the additional equations are required to complement the original equations, which is the limitation of the Newton-type predictor–corrector continuation method. Moreover, there exist a number of obstacles against efficient tracking the periodic solutions of nonlinear systems with multi parameters. Besides, the implementation of the continuation method faces difficulties for the isolated solution problem [36–38]. Indeed, the existence of isolated solution is an important hindrance by using the continuation method for detecting the isolated branch.

The stability problem of periodic solution is very essential and crucial for nonlinear dynamical system [39–41], and many papers investigating in general the stability of periodic solutions have been published [42,43]. In generally, there are two category approaches to analyze the stability of periodic solutions: time- and frequency-domain approaches. The major limitation of the time-domain stability analysis approach is that it cannot be used to analyze larger systems due to the computational requirement. Therefore, the frequency-domain stability analysis method is preferable and a number of publications about the frequency-domain stability analysis of periodic solutions can be found in studies. For example, Villa et al. [44] conducts stability analysis assessment in the frequency domain for a rotor bearing system. Recently, stability analysis of periodic solution has been extended to nonlinear systems with fraction order derivative in Ref. [13]. A deeper comparison of these stability methods is available in Ref. [45].

Most existing studies focus on strategies for analyzing the stability of periodic solutions and the stability analysis of quasi-periodic solution is scarcely available. For instance, the classic monodromy matrix algorithm in the time domain is extended to assess the asymptotic stability of quasi-periodic motions in Ref. [46]. The Floquet multipliers are computed through the interpolation of the state transition matrix for the perturbed system. However, the time integration process with a sufficiently small time step to ensure convergence is significantly time-consuming. After an extensive review on quasi-periodic motions, it is observed that a few papers have dealt with the stability of quasi-periodic motions and creating a method for analyzing the stability of quasi-periodic solutions is still an open question.

Our work provides two major contributions to the existing studies, namely an investigation of the stability analysis method for quasi-periodic solutions and an algorithm which integrates the reduced space gradient-based optimizer with the multi-dimensional harmonic balance method to follow the aperiodic solutions of nonlinear systems. To the best of our knowledge, this is the first attempt to solve the continuation problem by virtue of the nonlinear constraint optimization method. Furthermore, the stability of quasi-periodic solution is investigated in the frequency domain for the first time.

The remainder of this article is organized as follows. A proper optimization description of the continuation algorithm for quasi-periodic solutions is presented in Sect. 2. This is followed by the derivation of the stability and sensitivity analysis method in Sect. 3. Two numerical examples are conducted to examine the proposed method in Sect. 4. Finally, in Sect. 5, the main conclusions are highlighted, and some paths for future works are indicated.

2 The continuation method for quasi-periodic solutions of nonlinear systems

The mathematical formulations and implementation of the proposed continuation method of quasi-periodic solutions are described in this section and sensitivity analysis necessary for gradient-based optimization solver is also conducted.

2.1 The multi-dimensional harmonic balance method

The general equation of motion for nonlinear systems is expressed as

$$\boldsymbol{M}\ddot{\boldsymbol{u}} + \boldsymbol{C}\dot{\boldsymbol{u}} + \boldsymbol{K}\boldsymbol{u} + \boldsymbol{f}_{\text{nl}}(\boldsymbol{u}, t) = \boldsymbol{p}(t) \quad (1)$$

where \boldsymbol{M} , \boldsymbol{C} , and \boldsymbol{K} denote mass, damping, and stiffness matrices of nonlinear structures, respectively. The dots refer to the derivatives with respect to time t . \boldsymbol{u} , $\dot{\boldsymbol{u}}$, and $\ddot{\boldsymbol{u}}$ with N_d being the dimension are displacements, velocity, and acceleration response vectors, respectively. $\boldsymbol{f}_{\text{nl}}(\boldsymbol{u}, t)$ represents the vector of nonlinear restoring force and $\boldsymbol{p}(t)$ means the external force vector.

The multi-dimensional harmonic balance method approximates the unknown time function $\boldsymbol{u}(t)$ by a multiple Fourier series with finite terms which can be written as follows:

$$\begin{aligned} \boldsymbol{u}(t) &= \sum_{\boldsymbol{k}} [\boldsymbol{U}_{\boldsymbol{k}}^c \cos(\boldsymbol{k}, \boldsymbol{\omega})t + \boldsymbol{U}_{\boldsymbol{k}}^s \sin(\boldsymbol{k}, \boldsymbol{\omega})t] \\ &= \text{Real} ((\boldsymbol{\Theta} \otimes \boldsymbol{I}) \hat{\boldsymbol{U}}) = (\boldsymbol{E} \otimes \boldsymbol{I}) \boldsymbol{U} \end{aligned} \quad (2)$$

$$\boldsymbol{\Theta} = \begin{pmatrix} e^{2\pi\sqrt{-1}(\boldsymbol{k}^{-N_K}, \tau^1)} & \dots & e^{2\pi\sqrt{-1}(\boldsymbol{k}^{-1}, \tau^1)} & 1 & e^{2\pi\sqrt{-1}(\boldsymbol{k}^1, \tau^1)} & \dots & e^{2\pi\sqrt{-1}(\boldsymbol{k}^{N_K}, \tau^1)} \\ e^{2\pi\sqrt{-1}(\boldsymbol{k}^{-N_K}, \tau^2)} & \dots & e^{2\pi\sqrt{-1}(\boldsymbol{k}^{-1}, \tau^2)} & 1 & e^{2\pi\sqrt{-1}(\boldsymbol{k}^1, \tau^2)} & \dots & e^{2\pi\sqrt{-1}(\boldsymbol{k}^{N_K}, \tau^2)} \\ \vdots & \ddots & \vdots & \vdots & \vdots & \ddots & \vdots \\ e^{2\pi\sqrt{-1}(\boldsymbol{k}^{-N_K}, \tau^{N_\tau})} & \dots & e^{2\pi\sqrt{-1}(\boldsymbol{k}^{-1}, \tau^{N_\tau})} & 1 & e^{2\pi\sqrt{-1}(\boldsymbol{k}^1, \tau^{N_\tau})} & \dots & e^{2\pi\sqrt{-1}(\boldsymbol{k}^{N_K}, \tau^{N_\tau})} \end{pmatrix} \quad (4)$$

$$\boldsymbol{\Theta}^{-1} = \frac{1}{N_\tau} \begin{pmatrix} e^{2\pi\sqrt{-1}(\boldsymbol{k}^{-N_K}, \tau^1)} & e^{2\pi\sqrt{-1}(\boldsymbol{k}^{-N_K}, \tau^2)} & \dots & e^{2\pi\sqrt{-1}(\boldsymbol{k}^{-N_K}, \tau^{N_\tau})} \\ \vdots & \vdots & \ddots & \vdots \\ e^{2\pi\sqrt{-1}(\boldsymbol{k}^{-1}, \tau^1)} & e^{2\pi\sqrt{-1}(\boldsymbol{k}^{-1}, \tau^2)} & \dots & e^{2\pi\sqrt{-1}(\boldsymbol{k}^{-1}, \tau^{N_\tau})} \\ 1 & 1 & \dots & 1 \\ e^{2\pi\sqrt{-1}(\boldsymbol{k}^1, \tau^1)} & e^{2\pi\sqrt{-1}(\boldsymbol{k}^1, \tau^2)} & \dots & e^{2\pi\sqrt{-1}(\boldsymbol{k}^1, \tau^{N_\tau})} \\ \vdots & \vdots & \ddots & \vdots \\ e^{2\pi\sqrt{-1}(\boldsymbol{k}^{N_K}, \tau^1)} & e^{2\pi\sqrt{-1}(\boldsymbol{k}^{N_K}, \tau^2)} & \dots & e^{2\pi\sqrt{-1}(\boldsymbol{k}^{N_K}, \tau^{N_\tau})} \end{pmatrix} \quad (5)$$

where $\boldsymbol{U}_{\boldsymbol{k}}^c$ and $\boldsymbol{U}_{\boldsymbol{k}}^s$ in which the superscripts c and s indicate the cosine and sine terms, respectively, are the Fourier coefficients vectors. The sum is taken over

all combinations of $\boldsymbol{k} = [k_1, k_2, \dots, k_M]$ with $k_i = -N_H, -N_H + 1, \dots, -1, 0, 1, \dots, N_H$ where N_H is the chosen maximum order which represents the harmonic index-related combination vector. The vector $\boldsymbol{\omega} = [\omega_1, \omega_2, \dots, \omega_M]$ denotes the frequencies basis, and the dimensionless time basis vector is represented by $\boldsymbol{\tau} = [\tau_1, \tau_2, \dots, \tau_M]$ with $\tau_i = \omega_i t$. (\cdot) stands for the dot product

$$(\boldsymbol{k}, \boldsymbol{\omega}) = \sum_{i=1}^M k_i \omega_i \quad (3)$$

In Eq. (2), the multi-dimensional complex Fourier matrix $\boldsymbol{\Theta}$ and its inverse matrix $\boldsymbol{\Theta}^{-1}$ are detailed as follows:

where N_τ is the number of combination time points and $\sqrt{-1}$ is the imaginary unity. N_K specifies a finite set of multi-indices.

Analogously, the multi-dimensional real Fourier matrix \boldsymbol{E} and the corresponding Fourier transformation matrix \boldsymbol{E}^{-1} in Eq. (2) are expressed as:

$$\boldsymbol{E} = \begin{bmatrix} 1 \cos(2\pi(\boldsymbol{k}^1, \tau^1)) & \sin(2\pi(\boldsymbol{k}^1, \tau^1)) & \dots & \cos(2\pi(\boldsymbol{k}^{N_K}, \tau^1)) & \sin(2\pi(\boldsymbol{k}^{N_K}, \tau^1)) \\ 1 \cos(2\pi(\boldsymbol{k}^1, \tau^2)) & \sin(2\pi(\boldsymbol{k}^1, \tau^2)) & \dots & \cos(2\pi(\boldsymbol{k}^{N_K}, \tau^2)) & \sin(2\pi(\boldsymbol{k}^{N_K}, \tau^2)) \\ \vdots & \vdots & & \vdots & \vdots \\ 1 \cos(2\pi(\boldsymbol{k}^1, \tau^{N_\tau})) & \sin(2\pi(\boldsymbol{k}^1, \tau^{N_\tau})) & \dots & \cos(2\pi(\boldsymbol{k}^{N_K}, \tau^{N_\tau})) & \sin(2\pi(\boldsymbol{k}^{N_K}, \tau^{N_\tau})) \end{bmatrix} \quad (6)$$

$$\mathbf{E}^{-1} = \frac{2}{N_\tau} \begin{bmatrix} 1/2 & 1/2 & \cdots & 1/2 \\ \cos(2\pi(\mathbf{k}^1, \tau^1)) & \cos(2\pi(\mathbf{k}^1, \tau^2)) & \cdots & \cos(2\pi(\mathbf{k}^1, \tau^{N_\tau})) \\ \sin(2\pi(\mathbf{k}^1, \tau^1)) & \sin(2\pi(\mathbf{k}^1, \tau^2)) & \cdots & \sin(2\pi(\mathbf{k}^1, \tau^{N_\tau})) \\ \cos(2\pi(\mathbf{k}^2, \tau^1)) & \cos(2\pi(\mathbf{k}^2, \tau^2)) & \cdots & \cos(2\pi(\mathbf{k}^2, \tau^{N_\tau})) \\ \sin(2\pi(\mathbf{k}^2, \tau^1)) & \sin(2\pi(\mathbf{k}^2, \tau^2)) & \cdots & \sin(2\pi(\mathbf{k}^2, \tau^{N_\tau})) \\ \vdots & \vdots & \ddots & \vdots \\ \cos(2\pi(\mathbf{k}^{N_K}, \tau^1)) & \cos(2\pi(\mathbf{k}^{N_K}, \tau^2)) & \cdots & \cos(2\pi(\mathbf{k}^{N_K}, \tau^{N_\tau})) \\ \sin(2\pi(\mathbf{k}^{N_K}, \tau^1)) & \sin(2\pi(\mathbf{k}^{N_K}, \tau^2)) & \cdots & \sin(2\pi(\mathbf{k}^{N_K}, \tau^{N_\tau})) \end{bmatrix} \quad (7)$$

The vectors of selected multi-indices for the multi-dimensional Fourier series are defined as

$$\hat{\mathbf{U}} = \left[(\mathbf{U}_{\mathbf{k}^{N_K}}^c - \sqrt{-1}\mathbf{U}_{\mathbf{k}^{N_K}}^s)^T \right. \\ \cdots (\mathbf{U}_0)^T (\mathbf{U}_{\mathbf{k}^1}^c - \sqrt{-1}\mathbf{U}_{\mathbf{k}^1}^s)^T \\ \cdots (\mathbf{U}_{\mathbf{k}^{N_K}}^c - \sqrt{-1}\mathbf{U}_{\mathbf{k}^{N_K}}^s)^T \left. \right]^T \\ \mathbf{U} = \left[(\mathbf{U}_0)^T (\mathbf{U}_{\mathbf{k}^1}^c)^T (\mathbf{U}_{\mathbf{k}^1}^s)^T \cdots (\mathbf{U}_{\mathbf{k}^l}^c)^T (\mathbf{U}_{\mathbf{k}^l}^s)^T \right. \\ \cdots (\mathbf{U}_{\mathbf{k}^{N_K}}^c)^T (\mathbf{U}_{\mathbf{k}^{N_K}}^s)^T \left. \right]^T \quad (8)$$

In the present work, a strategy similar to Ref. [46] is adopted to define the subset of Fourier basis truncation terms. The selected harmonic indices with $N_H = 5$ are plotted in Fig. 1 if the vector $\mathbf{k} = [k_1 k_2]$ contains two elements. In Fig. 1, the absolute value of k_i is smaller than or equal to N_H , which leads to the presence of $2N_K + 1$ harmonic terms. The choice of N_H depends on the application. A large value of N_H increases the accuracy to approximate quasi-periodic solution but makes the optimization process more complex and penalizes robustness. The images of \mathbf{E} and \mathbf{E}^{-1} in Eqs. (6) and (7) associated with the selected harmonic in Fig. 1 are depicted in Fig. 2. Using the orthonormality property of the harmonic functions, the matrix products of $\Theta^{-1}\Theta$ and $\mathbf{E}^{-1}\mathbf{E}$ are diagonal, which are plotted in Fig. 3.

Plugging Eq. (2) into Eq. (1) and applying the Galerkin procedure yield the following nonlinear function

$$\mathbf{g}(\mathbf{U}, \omega) = \mathbf{A}(\omega)\mathbf{U} + \mathbf{b}(\mathbf{U}, \omega) = \mathbf{0} \quad (9)$$

where $\mathbf{b} = \left[(\mathbf{C}_0)^T (\mathbf{C}_{\mathbf{k}^1}^c)^T (\mathbf{S}_{\mathbf{k}^1}^s)^T \cdots (\mathbf{C}_{\mathbf{k}^l}^c)^T (\mathbf{S}_{\mathbf{k}^l}^s)^T \cdots (\mathbf{C}_{\mathbf{k}^{N_K}}^c)^T (\mathbf{S}_{\mathbf{k}^{N_K}}^s)^T \right]^T$ in which the superscript T denotes matrix transpose corresponds to the Fourier coefficients of the nonlinear forcing term and the external force; $\mathbf{A}(\omega)$ is derived as

$$\mathbf{A} = \nabla^2 M + \nabla C + \text{diag}(K, K, \dots, K), \nabla$$

$$= \text{diag}(\mathbf{0}, \nabla_1, \nabla_2, \dots, \nabla_{N_K}), \nabla_l$$

$$= (\mathbf{k}^l, \omega) \begin{bmatrix} 0 & 1 \\ -1 & 0 \end{bmatrix} \\ \mathbf{A} = \text{diag} \left(K, \begin{bmatrix} K - (k^1, \omega)^2 M & (k^1, \omega) C \\ -(k^1, \omega) C & K - (k^1, \omega)^2 M \end{bmatrix}, \right. \\ \cdots, \begin{bmatrix} K - (k^l, \omega)^2 M & (k^l, \omega) C \\ -(k^l, \omega) C & K - (k^l, \omega)^2 M \end{bmatrix}, \\ \cdots, \left. \begin{bmatrix} K - (k^{N_K}, \omega)^2 M & (k^{N_K}, \omega) C \\ -(k^{N_K}, \omega) C & K - (k^{N_K}, \omega)^2 M \end{bmatrix} \right) \quad (10)$$

Equation (9) which can be solved by using the gradient-based optimization algorithm provides $N_d(2N_K + 1)$ equations, but there are $N_d(2N_K + 1) + M$ unknowns to determine (the additional unknown being the frequency vector ω). The key idea of the multi-dimensional harmonic balance method is to find the unknown harmonic coefficients \mathbf{U} and ω in Eq. (9). The main computational bottleneck is the evaluation of the unknown coefficients \mathbf{b} in Eq. (9), which can be deduced from the multi-dimensional Fourier transform of the time domain nonlinear force. Fortunately, the nonlinear force can be

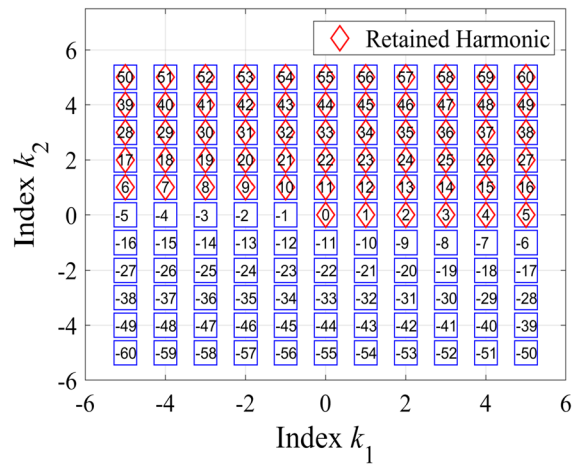


Fig. 1 The selected harmonic index

Fig. 2 The multi-dimensional Fourier matrix and its inverse matrix

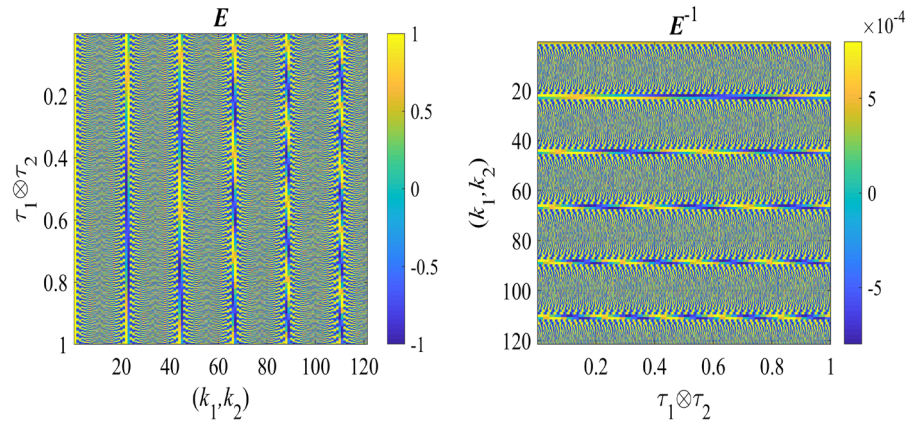
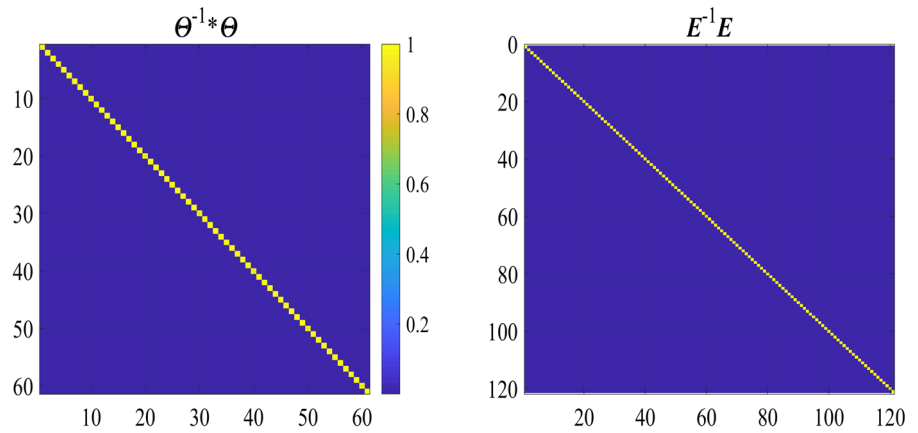


Fig. 3 The matrix products of multi-dimensional Fourier related matrix



derived from an iterative solution of $\mathbf{u}(t)$ being the inverse multi-dimensional Fourier transform of \mathbf{U} . This alternative frequency time domain method is summed up by the following scheme [47]:

$$\mathbf{U} \xrightarrow{\mathbf{E}} \mathbf{u}(t) \Rightarrow \mathbf{f}_{\text{nl}}(\mathbf{u}, t) \xrightarrow{\mathbf{E}^{-1}} \mathbf{b}(\mathbf{U}, \boldsymbol{\omega}). \quad (11)$$

2.2 Continuation problem formulation

Based on the quasi-periodic representation of $\mathbf{u}(t)$, the frequency $\boldsymbol{\omega}$ and the Fourier coefficients are considered as optimization variables. As the conventional multi-dimensional harmonic balance method is used, Eq. (9) is a set of nonlinear equations being directly solved by the root-finding method or the continuation procedure. However, the application of the root-finding method requires that the number of unknown variables is equal to the number of nonlinear equations, that is, Eq. (9) is a well-defined nonlinear system. Nevertheless, the nonlinear algebraic equations in Eq. (9) are underdefined and the root-finding algorithm cannot be used

to determine the unknown Fourier coefficients and $\boldsymbol{\omega}$. Therefore, constraint equation(s) must be added to get a square system for the continuation method

The solutions of Eq. (9) are solved and tracked by the predictor–corrector continuation method which consists of the prediction and correction steps. Starting from the known solutions such as \mathbf{x}_{i-1} and \mathbf{x}_i , the prediction $\mathbf{x}_{i+1}^{\text{pred}}$ at the prediction step is produced based on the prediction method such as the secant method

$$\mathbf{x}_{i+1}^{\text{pred}} = \mathbf{x}_i + \Delta h^i \frac{\mathbf{x}_i - \mathbf{x}_{i-1}}{\|(\mathbf{x}_i - \mathbf{x}_{i-1})\|} \quad (12)$$

where $\mathbf{x}_i = \left\{ (\mathbf{U}^i)^T, (\boldsymbol{\omega}^i)^T \right\}^T$ and Δh^i is the continuation step size $\|\bullet\|$ denotes the norm of \bullet .

The prediction $\mathbf{x}_{i+1}^{\text{pred}}$ which is used as the initial point for the correction step must be corrected using the root-finding algorithm since the prediction will not in general satisfy the harmonic balance equations. In order to apply the Newton like root-finding method, extra equation(s) should be appended to Eq. (9). One way to impose the appended equation(s) is to add the following

approximation of the curve abscissa increment which measures the distance between two points \mathbf{x} and \mathbf{x}_i

$$\Delta s^i = \sqrt{(\mathbf{U} - \mathbf{U}^i)^T (\mathbf{U} - \mathbf{U}^i) + (\boldsymbol{\omega} - \boldsymbol{\omega}^i)^2} = 0 \quad (13)$$

where Δs^i denotes the step increment.

In addition, the harmonic balance equations in Eq. (9) can be complemented with the so-called pseudo-arclength condition

$$(\mathbf{U} - \mathbf{U}^i)^T (\mathbf{U} - \mathbf{U}^i) + (\boldsymbol{\omega} - \boldsymbol{\omega}^i)^T (\boldsymbol{\omega} - \boldsymbol{\omega}^i) = 0 \quad (14)$$

Unlike the traditional implementation of the corrected step for the continuation method, the prediction solution is corrected by using the nonlinear constraints optimization method in the following. Since an intrinsic step of the continuation method is a minimization process, the objective function in the present formulation is selected to minimize the residual of Eq. (14) with respect to the unknown optimization variables $\mathbf{x} = \{\mathbf{U}, \boldsymbol{\omega}\}^T$, while the harmonic balance equations in Eq. (9) should be satisfied. Hence, Eqs. (9) and (14) are to be combined and solved simultaneously in order to solve the quasi-periodic solutions of nonlinear systems. Therefore, the presented correction scheme for the continuation of quasi-periodic solution is formulated as the minimization problem with harmonic balance constraint equations as follows:

$$\begin{aligned} \min f(\mathbf{x}) &= f(\mathbf{U}, \boldsymbol{\omega}) = (\mathbf{U} - \mathbf{U}^i)^T (\mathbf{U} - \mathbf{U}^i) \\ &\quad + (\boldsymbol{\omega} - \boldsymbol{\omega}^i)^T (\boldsymbol{\omega} - \boldsymbol{\omega}^i) \\ \text{s.t. } &\left\{ \begin{array}{l} \mathbf{g}(\mathbf{x}) = \mathbf{A}(\boldsymbol{\omega})\mathbf{U} + \mathbf{b}(\mathbf{U}, \boldsymbol{\omega}) = \mathbf{0} \\ \mathbf{x}_L \leq \mathbf{x} \leq \mathbf{x}_U \end{array} \right. \end{aligned} \quad (15)$$

where $\mathbf{g}(\mathbf{x})$ means the nonlinear equality constraints. Inequality constraints \mathbf{x}_L and \mathbf{x}_U refer to the lower and upper bounds, respectively.

The prediction step in Eq. (14) and the correction step in Eq. (15) are applied repeatedly to trace quasi-periodic solution over the continuation parameter space. The proposed continuation algorithm is based on a combination of several ingredients: the multi-dimensional harmonic balance method, the reduced space SQP method, and the continuation strategy. The gradient optimization algorithm is employed to solve Eq. (15). However, the sensitivity information with respect to unknown variables is required to find searching direction for optimization updates. Therefore, the

sensitivities of the objective and constraint functions should be derived.

2.3 The gradients of the nonlinear equality constraints

The derivatives for both objective and constraint functions with respect to the optimization variables are needed in order to efficiently solve Eq. (15) through a gradient-based optimization method. Furthermore, an accurate Jacobian matrix of the harmonic balance equations in Eq. (9) is required to undertake stability analysis of quasi-periodic solution. Since the sensitivity of the objective function in Eq. (15) is straightforward, no explicit expression will be given here. In the following, the gradients of the nonlinear equality constraints in Eq. (15) are derived.

From Eq. (15), the following expression for Jacobian matrix can be obtained

$$\frac{\partial \mathbf{g}(\mathbf{x})}{\partial \mathbf{U}} = \mathbf{A} + \frac{\partial \mathbf{b}}{\partial \mathbf{U}} \quad (16)$$

By utilizing the relation in Eq. (11) for the previous expression, the gradient $\frac{\partial \mathbf{b}}{\partial \mathbf{U}}$ can be derived by using the chain rule of differentiation:

$$\begin{aligned} \frac{\partial \mathbf{b}}{\partial \mathbf{U}} &= \frac{\partial \mathbf{b}}{\partial \mathbf{f}_{\text{nl}}(\mathbf{u}, \tau)} \frac{\partial \mathbf{f}_{\text{nl}}(\mathbf{u}, \tau)}{\partial \mathbf{u}(\tau)} \frac{\partial \mathbf{u}(\tau)}{\partial \mathbf{U}} \\ &= (\mathbf{E}^{-1} \otimes \mathbf{I}) \left(\frac{\partial \mathbf{f}_{\text{nl}}(\mathbf{u}, \tau)}{\partial \mathbf{u}(\tau)} \right) (\mathbf{E} \otimes \mathbf{I}) \end{aligned} \quad (17)$$

where the dimensional of the identity matrix \mathbf{I} is equal to the number of Dof N_d and other matrices are given by

$$\frac{\partial \mathbf{f}_{\text{nl}}(\mathbf{u}, \tau)}{\partial \mathbf{u}(\tau)} = \text{diagblk} \left(\frac{\partial \mathbf{f}_{\text{nl}}(\mathbf{u}, \tau)}{\partial \mathbf{u}(\tau)} \Big|_{\tau_1}, \frac{\partial \mathbf{f}_{\text{nl}}(\mathbf{u}, \tau)}{\partial \mathbf{u}(\tau)} \Big|_{\tau_2}, \dots, \frac{\partial \mathbf{f}_{\text{nl}}(\mathbf{u}, \tau)}{\partial \mathbf{u}(\tau)} \Big|_{\tau_{N_\tau}} \right) \quad (18)$$

The sensitivity analysis related to $\frac{\partial \mathbf{g}(\mathbf{x})}{\partial \bar{x}_i}$ can be calculated easily. For instance, $\frac{\partial \mathbf{g}(\mathbf{x})}{\partial \omega_i}$ is calculated as follows:

$$\begin{aligned} \frac{\partial \mathbf{A}}{\partial \omega_i} &= \text{diag} \left(0, \begin{bmatrix} -2(k^1, \omega)k_i^1 \mathbf{M} & k_i^1 \mathbf{C} \\ -k_i^1 \mathbf{C} & -2(k^1, \omega)k_i^1 \mathbf{M} \end{bmatrix}, \dots, \right. \\ &\quad \left. \begin{bmatrix} -2(k^{N_K}, \omega)k_i^{N_K} \mathbf{M} & k_i^{N_K} \mathbf{C} \\ -k_i^{N_K} \mathbf{C} & -2(k^{N_K}, \omega)k_i^{N_K} \mathbf{M} \end{bmatrix} \right) \end{aligned} \quad (19)$$

By incorporating these gradient formulas into a gradient-based optimization method, the nonlinear programming problem in Eq. (15) can be solved.

2.4 The reduced space sequential quadratic programming method for solving the constrained optimization problem

In the following, the reduced space sequential quadratic programming (SQP) methodology is adopted and reviewed to solve the nonlinear equality constrained optimization problem in Eq. (15). The basic idea of the reduced space SQP method is to model Eq. (15) at the current iteration point \mathbf{x}_k by a quadratic programming (QP) subproblem:

$$\begin{aligned} \min & [\nabla f(\mathbf{x}_k)]^T \mathbf{d}_k + \frac{1}{2} \mathbf{d}_k^T \mathbf{H}_k \mathbf{d}_k \\ \text{s.t. } & \left\{ \begin{array}{l} \mathbf{g}(\mathbf{x}_k) + [\nabla \mathbf{g}(\mathbf{x}_k)]^T \mathbf{d}_k = \mathbf{0} \\ \mathbf{x}_L \leq \mathbf{x}_k + \mathbf{d}_k \leq \mathbf{x}_U \end{array} \right. \end{aligned} \quad (20)$$

in which $\mathbf{H}_k \in R^{N \times N}$ with N being the dimension of \mathbf{x} is the approximation of the Hessian matrix of the Lagrangian function, $L(\mathbf{x}) = f(\mathbf{x}) + \lambda \mathbf{g}(\mathbf{x})$ where λ is the Lagrangian multiplier. The solution \mathbf{d}_k for this QP subproblem represents the search direction. The bounds of \mathbf{x} are included as the general constraints $\mathbf{g}(\mathbf{x})$. The symbol ∇ denotes the gradient operator.

Within the reduced space SQP method, the search direction \mathbf{d}_k can be expressed as the combination of the range space component \mathbf{d}_k^Y and the null space component \mathbf{d}_k^Z :

$$\mathbf{d}_k = \mathbf{Y}_k \mathbf{d}_k^Y + \mathbf{Z}_k \mathbf{d}_k^Z \quad (21)$$

where \mathbf{Y}_k with a size of $N \times M$ corresponds to the range space matrix of $\nabla \mathbf{g}(\mathbf{x}_k)$ while the columns of $\mathbf{Z}_k \in R^{N \times (N-M)}$ span the null space of $[\nabla \mathbf{g}(\mathbf{x}_k)]^T$. M represents the size of $\mathbf{g}(\mathbf{x})$.

By inserting Eq. (21) into Eq. (20) and utilizing the orthonormality property $[\nabla \mathbf{g}(\mathbf{x}_k)]^T \mathbf{Z}_k = \mathbf{0}$, dependent variables $\mathbf{d}_k^Y = -\{[\nabla \mathbf{g}(\mathbf{x}_k)]^T \mathbf{Y}_k\}^{-1} \mathbf{g}(\mathbf{x}_k)$ in the range space can be eliminated from the nonlinear equality constraints and the following bound constraint optimization problem is obtained:

$$\begin{aligned} \min & \left(\mathbf{Z}_k^T \nabla f(\mathbf{x}_k) + \frac{1}{2} \mathbf{Z}_k^T \mathbf{H}_k \mathbf{Y}_k \mathbf{d}_k^Y \right) \mathbf{d}_k^Y \\ \text{s.t. } & \mathbf{x}_L \leq \mathbf{x}_k + \mathbf{Y}_k \mathbf{d}_k^Y + \mathbf{Z}_k \mathbf{d}_k^Z \leq \mathbf{x}_U \end{aligned} \quad (22)$$

where \mathbf{d}_k^Z represents the independent optimization variables. The deduction of Eq. (22) can be seen in detail in Ref. [14]. A detailed review of the reduced space SQP approach is available in Refs. [48, 49].

Coupling the nonlinear constraints optimization method and the multi-dimensional harmonic balance approach with the numerical parameter continuation method, a continuation approach for tracking the quasi-periodic solutions is presented. The continuation of quasi-periodic solutions is achieved by virtue of the nonlinear constraint optimization method rather than the root-finding approach, thus offering flexibility to avoid the computational requirement with the use of the Newton–Raphson method in which the number of nonlinear equations is required to be equal to that of the unknowns. Once the unknown quasi-periodic solutions are obtained, the stability of the aperiodic solutions should be estimated.

3 Stability analysis for quasi-periodic solutions of nonlinear systems

Obtaining stability boundaries is vital to study the effects of structural parameters on the dynamic characteristic of nonlinear systems. The approach to be outlined in this section seeks to determine the stability of quasi-periodic solutions of nonlinear systems. With the help of the Floquet theory, the stability analysis is performed using the concept of superimposing a small disturbance around known quasi-periodic solution. The generalized eigenvalue problem is constructed and solved to determine the stability of quasi-periodic solution.

3.1 Stability assessment for quasi-periodic solutions of nonlinear systems

The idea of the proposed method is based on considering a perturbation from the steady-state solution and then the stability of the steady-state solution is determined by examining the stability of the perturbation. Let $\mathbf{L}e^{\lambda t}$ with the Fourier coefficients $\tilde{\mathbf{U}} = \left[(\tilde{\mathbf{U}}_0)^T \ (\tilde{\mathbf{U}}_k^c)^T \ (\tilde{\mathbf{U}}_k^s)^T \ \dots \ (\tilde{\mathbf{U}}_{k^{NK}}^c)^T \ (\tilde{\mathbf{U}}_{k^{NK}}^s)^T \right]^T$ be a small perturbation for the known quasi-periodic solution \mathbf{u}_0 of Eq. (1). In the following, Eq. (1) is evaluated by using $\mathbf{u} = \mathbf{u}_0 + \mathbf{L}e^{\lambda t}$ to derive the stability method. Introducing the perturbation $\mathbf{L}e^{\lambda t}$ into Eq. (1) yields the stability information. By plugging $\mathbf{u} = \mathbf{u}_0 + \mathbf{L}e^{\lambda t}$ into Eq. (1) and replacing the expressions for $\dot{\mathbf{u}}$ and $\ddot{\mathbf{u}}$, the stability analysis problem can be formulated as follows:

$$\begin{aligned} \mathbf{M}\ddot{\mathbf{u}}_0 + \mathbf{C}\dot{\mathbf{u}}_0 + \mathbf{K}\mathbf{u}_0 + \mathbf{f}_{\text{nl}}(\mathbf{u}_0 + \mathbf{L}e^{\lambda t}) - \mathbf{p}(t) \\ + e^{\lambda t} \left\{ \lambda^2 \mathbf{M}\mathbf{L} + \lambda \left(2\mathbf{M}\dot{\mathbf{L}} + \mathbf{C}\mathbf{L} \right) \right. \\ \left. + \left(\mathbf{M}\ddot{\mathbf{L}} + \mathbf{C}\dot{\mathbf{L}} + \mathbf{K} \right) \right\} \approx 0 \end{aligned} \quad (23)$$

Using the Fourier series expansion of Eq. (2), the previous equation of motion in the time domain can be recast in the frequency domain

$$\mathbf{A}\bar{\mathbf{U}} + (\lambda^2 \mathbf{J}_2 + \lambda \mathbf{J}_1 + \mathbf{A})\bar{\mathbf{U}}e^{\lambda t} + \mathbf{b}(\bar{\mathbf{U}} + e^{\lambda t}\tilde{\mathbf{U}}) = 0 \quad (24)$$

where $\bar{\mathbf{U}}$ which satisfies the relation $\mathbf{A}\bar{\mathbf{U}} + \mathbf{b}(\bar{\mathbf{U}}) = 0$ represents the Fourier coefficients associated with \mathbf{u}_0 .

According to the Floquet theory, the equilibrium position corresponds to the trivial solution of Eq. (23) and the stability of the trivial solution is determined by Eq. (24). Thus the study of the stability of quasi-periodic solution is transformed into the stability analysis of null solution of Eq. (24). Based on the Taylor expansion of $\mathbf{b}(\bar{\mathbf{U}} + e^{\lambda t}\tilde{\mathbf{U}})$, the trivial solution can be determined by following generalized eigenvalue problem

$$[\lambda^2 \mathbf{J}_2 + \lambda \mathbf{J}_1 + \mathbf{J}_0] \psi = 0 \quad (25)$$

where the detailed matrices \mathbf{J}_0 and \mathbf{J}_1 are given by:

$$\mathbf{J}_0 = \mathbf{A} + \frac{\partial \mathbf{b}}{\partial \mathbf{U}} \quad (26)$$

$$\begin{aligned} \mathbf{J}_1 = \text{diagblk} \left(\mathbf{C}, \begin{bmatrix} \mathbf{C} & 2(\mathbf{k}^1, \omega)\mathbf{M} \\ -2(\mathbf{k}^1, \omega)\mathbf{M} & \mathbf{C} \end{bmatrix}, \dots, \right. \\ \left. \begin{bmatrix} \mathbf{C} & 2(\mathbf{k}^{N_K}, \omega)\mathbf{M} \\ -2(\mathbf{k}^{N_K}, \omega)\mathbf{M} & \mathbf{C} \end{bmatrix} \right) \quad (27) \end{aligned}$$

$$\mathbf{J}_2 = \text{diagblk}(\mathbf{M}, \mathbf{M}, \dots, \mathbf{M}) \quad (28)$$

Equation (25) which is a quadratic eigenvalue problem provides information on the stability of quasi-periodic solution. In the following, the standard eigenvalue solution is used rather than the generalized one to compute the eigenvalues and eigenvectors because of its higher accuracy and computational performance. In order to construct the state-space representation of the standard eigenvalue problem, the eigenvalue equation of Eq. (25) is reformulated as

$$\begin{aligned} \bar{\mathbf{A}}\bar{\psi}_j &= \lambda_j \bar{\mathbf{B}}\bar{\psi}_j \\ \bar{\phi}_j^T \bar{\mathbf{A}} &= \lambda_j \bar{\phi}_j^T \bar{\mathbf{B}} \end{aligned} \quad (29)$$

where $\bar{\phi}_j$ and $\bar{\psi}_j$ are the j th left and right eigenvectors associated with eigenvalue λ_j , respectively. The matrices $\bar{\mathbf{A}}$ and $\bar{\mathbf{B}}$ are given by

$$\bar{\mathbf{A}} = \begin{bmatrix} \mathbf{I} & 0 \\ 0 & -\mathbf{J}_2^T \end{bmatrix}, \quad \bar{\mathbf{B}} = \begin{bmatrix} 0 & \mathbf{I} \\ \mathbf{J}_0^T & \mathbf{J}_1^T \end{bmatrix} \quad (30)$$

Although the eigenvalue problem is now first order, the size of the eigenvalue problem in Eq. (29) has doubled, as a result doubling the size of the eigenvalue and eigenvector matrices. According to the Floquet theory the stability of quasi-periodic solution is examined on a basis of eigenvalues resulting from the eigenvalue problem of Eq. (29). Following the approach in Ref. [38], the eigenvalues λ_j^s with the smallest image part which are also called the Floquet multipliers are selected to identify the stability of quasi-periodic solution. Unstable quasi-periodic solution will have eigenvalues with positive real part, while stable one will have eigenvalues with negative real part.

3.2 Sensitivity analysis for the stability factors of quasi-periodic solutions

By virtue of the generalized eigenvalue problem in Eq. (25), the sensitivity of the stability factor λ_j^s with respect to the influence parameter p can be derived. In the following, sensitivity analysis for the stability factor is performed.

To evaluate $\frac{\partial \lambda_j}{\partial p}$, the expression in Eq. (25) is differentiated with respect to p using the Taylor's series expansion

$$\begin{aligned} &\left[\lambda_j^2 \frac{\partial \mathbf{J}_2}{\partial p} + \lambda_j \frac{\partial \mathbf{J}_1}{\partial p} + \frac{\partial \mathbf{J}_0}{\partial p} \right] \psi_j \\ &+ [2\lambda_j \mathbf{J}_2 + \mathbf{J}_1] \psi_j \frac{\partial \lambda_j}{\partial p} = 0 \end{aligned} \quad (31)$$

Using the expression in Eq. (31), the derivative $\frac{\partial \lambda_j}{\partial p}$ is obtained as

$$\frac{\partial \lambda_j}{\partial p} = - \frac{\phi_j^T \left(\lambda_j^2 \frac{\partial \mathbf{J}_2}{\partial p} + \lambda_j \frac{\partial \mathbf{J}_1}{\partial p} + \frac{\partial \mathbf{J}_0}{\partial p} \right) \psi_j}{\phi_j^T (2\lambda_j \mathbf{J}_2 + \mathbf{J}_1) \psi_j} \quad (32)$$

In accordance with Eq. (32), the gradient of $\frac{\partial \lambda_j}{\partial U_{k'}^{c(s)}}$ is a vector with elements given by

$$\frac{\partial \lambda_j}{\partial U_{k'}^{c(s)}} = - \frac{\left(\phi_j^T \frac{\partial \mathbf{J}_0}{\partial U_{k'}^{c(s)}} \psi_j \right)}{\phi_j^T (2\lambda_j \mathbf{J}_2 + \mathbf{J}_1) \psi_j} \quad (33)$$

In order to calculate $\frac{\partial \mathbf{J}_0}{\partial U_{k'}^{c(s)}}$ in Eqs. (33), (17) can be directly differentiated with respect to $U_{k'}^{c(s)}$:

$$\frac{\partial \mathbf{J}_0}{\partial \mathbf{U}_{k^l}^{c(s)}} = \left(\frac{\partial \left(\frac{\partial b}{\partial U} \right)}{\partial \mathbf{U}_{k^l}^{c(s)}} \right) \quad (34)$$

Substituting Eq. (17) into Eq. (34) and taking the derivatives with respect to $\mathbf{U}_{k^l}^{c(s)}$ yields sensitivity required by Eq. (34)

$$\frac{\partial \left(\frac{\partial b}{\partial U} \right)}{\partial \mathbf{U}_{k^l}^{c(s)}} = (\mathbf{E}^{-1} \otimes \mathbf{I}) \left(\frac{\partial \left(\frac{\partial f_{nl}(\mathbf{u}, \tau)}{\partial \mathbf{u}(\tau)} \right)}{\partial \mathbf{U}_{k^l}^{c(s)}} \right) (\mathbf{E} \otimes \mathbf{I}) \quad (35)$$

The evaluation of $\frac{\partial \left(\frac{\partial b}{\partial U} \right)}{\partial \mathbf{U}_{k^l}^{c(s)}}$ in Eq. (35) still requires to obtain $\frac{\partial \left(\frac{\partial f_{nl}(\mathbf{u}, \tau)}{\partial \mathbf{u}(\tau)} \right)}{\partial \mathbf{U}_{k^l}^{c(s)}}$. Using the Leibniz's rule, differentiating $\frac{\partial f_{nl}(\mathbf{u}, \tau)}{\partial \mathbf{u}(\tau)}$ with respect to $\mathbf{U}_{k^l}^{c(s)}$ yields

$$\frac{\partial \left(\frac{\partial f_{nl}(\mathbf{u}, \tau)}{\partial \mathbf{u}(\tau)} \right)}{\partial \mathbf{U}_{k^l}^{c(s)}} = \frac{\partial \left(\frac{\partial f_{nl}(\mathbf{u}, \tau)}{\partial \mathbf{u}(\tau)} \right)}{\partial \mathbf{u}(\tau)} \frac{\partial \mathbf{u}(\tau)}{\partial \mathbf{U}_{k^l}^{c(s)}} \quad (36)$$

In Eq. (36), differentiations of $\mathbf{u}(\tau)$ with respect to $\mathbf{U}_{k^l}^{c(s)}$ are derived by virtue of Eq. (2). Therefore, the final expressions of $\frac{\partial \left(\frac{\partial f_{nl}(\mathbf{u}, \tau)}{\partial \mathbf{u}(\tau)} \right)}{\partial \mathbf{U}_{k^l}^{c(s)}}$ are derived and given below:

$$\begin{aligned} & \frac{\partial \left(\frac{\partial f_{nl}(\mathbf{u}, \tau)}{\partial \mathbf{u}(\tau)} \right)}{\partial \mathbf{U}_{k^l}^c} \\ &= \text{diagblk} \left(\frac{\partial \left(\frac{\partial f_{nl}(\mathbf{u}, \tau)}{\partial \mathbf{u}(\tau)} \right)}{\partial \mathbf{u}(\tau)} \Bigg|_{\tau_1} \cos \left(2\pi \left(\mathbf{k}^l, \tau^1 \right) \right), \right. \\ & \quad \left. \frac{\partial \left(\frac{\partial f_{nl}(\mathbf{u}, \tau)}{\partial \mathbf{u}(\tau)} \right)}{\partial \mathbf{u}(\tau)} \Bigg|_{\tau_2} \cos \left(2\pi \left(\mathbf{k}^l, \tau^2 \right) \right), \dots, \right. \\ & \quad \left. \frac{\partial \left(\frac{\partial f_{nl}(\mathbf{u}, \tau)}{\partial \mathbf{u}(\tau)} \right)}{\partial \mathbf{u}(\tau)} \Bigg|_{\tau^{N_\tau}} \cos \left(2\pi \left(\mathbf{k}^l, \tau^{N_\tau} \right) \right) \right) \quad (37) \\ & \frac{\partial \left(\frac{\partial f_{nl}(\mathbf{u}, \tau)}{\partial \mathbf{u}(\tau)} \right)}{\partial \mathbf{U}_{k^l}^s} \\ &= \text{diagblk} \left(\frac{\partial \left(\frac{\partial f_{nl}(\mathbf{u}, \tau)}{\partial \mathbf{u}(\tau)} \right)}{\partial \mathbf{u}(\tau)} \Bigg|_{\tau_1} \sin \left(2\pi \left(\mathbf{k}^l, \tau^1 \right) \right), \right. \\ & \quad \left. \frac{\partial \left(\frac{\partial f_{nl}(\mathbf{u}, \tau)}{\partial \mathbf{u}(\tau)} \right)}{\partial \mathbf{u}(\tau)} \Bigg|_{\tau_2} \sin \left(2\pi \left(\mathbf{k}^l, \tau^2 \right) \right), \dots, \right. \end{aligned}$$

$$\frac{\partial \left(\frac{\partial f_{nl}(\mathbf{u}, \tau)}{\partial \mathbf{u}(\tau)} \right)}{\partial \mathbf{u}(\tau)} \Bigg|_{\tau^{N_\tau}} \sin \left(2\pi \left(\mathbf{k}^l, \tau^{N_\tau} \right) \right) \quad (38)$$

Furthermore, it is obvious that the gradient of the stability factors with respect to ω_i is readily obtained from Eq. (32)

$$\frac{\partial \lambda_j}{\partial \omega_i} = -\frac{\phi_j^T \left(\lambda_j^2 \frac{\partial J_2}{\partial \omega_i} + \lambda_j \frac{\partial J_1}{\partial \omega_i} + \frac{\partial J_0}{\partial \omega_i} \right) \psi_j}{\phi_j^T [2\lambda_j J_2 + J_1] \psi_j} \quad (39)$$

where the related matrices are detailed as follows:

$$\begin{aligned} \frac{\partial J_1}{\partial \omega_i} &= \text{diag} \left(0, 2k_i^1 \begin{bmatrix} \mathbf{0} & \mathbf{M} \\ -\mathbf{M} & \mathbf{0} \end{bmatrix}, \dots, 2k_i^{N_K} \begin{bmatrix} \mathbf{0} & \mathbf{M} \\ -\mathbf{M} & \mathbf{0} \end{bmatrix} \right) \\ \frac{\partial J_0}{\partial \omega_i} &= \text{diag} \left(0, \begin{bmatrix} -2(k^1, \omega) k_i^1 \mathbf{M} & k_i^1 \mathbf{C} \\ -k_i^1 \mathbf{C} & -2(k^1, \omega) k_i^1 \mathbf{M} \end{bmatrix}, \dots, \right. \\ & \quad \left. \begin{bmatrix} -2(k^{N_K}, \omega) k_i^{N_K} \mathbf{M} & k_i^{N_K} \mathbf{C} \\ -k_i^{N_K} \mathbf{C} & -2(k^{N_K}, \omega) k_i^{N_K} \mathbf{M} \end{bmatrix} \right) \quad (40) \end{aligned}$$

A new stability analysis method for quasi-periodic solutions of nonlinear systems is presented in this section which gathers the theoretical derivations for the proposed stability analysis approach. The stability of quasi-periodic solution is identified by solving the standard eigenvalue problem resulted from the application of the perturbation theory to the harmonic balance equations and further treatments of the sensitivity of the stability factor are also derived.

4 Application to select nonlinear dynamical systems

This section is dedicated to the validation and assessment of the proposed method. Two representative examples are demonstrated.

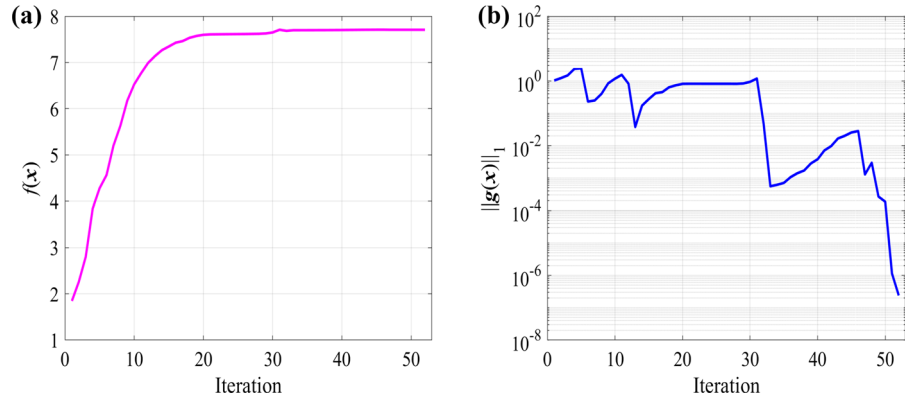
4.1 Duffing oscillator

A classical Duffing oscillator is considered as the first example to verify the efficiency and accuracy of the proposed methods. The equation of motion of the harmonically forced Duffing oscillator is described below:

$$\ddot{u} + 2\zeta \dot{u} + u + \gamma u^3 = f_1 \sin(\omega_1 t) + f_2 \sin(\omega_2 t) \quad (41)$$

where ζ and γ denote the damping coefficient and the nonlinear stiffness coefficient, respectively. f_1 and f_2 represent the force amplitudes. ω_1 and $\omega_2 = \frac{\omega_1}{\sqrt{2}}$ mean

Fig. 4 Evolution of the optimization iteration for the resonant peak quasi-periodic solution



the two excitation frequencies. In all the following tests, unless otherwise specified, the structural parameters of Eq. (41) are adopted as the same as those in Ref. [46]: $\zeta = 0.1$, $\gamma = 0.2$, $f_1 = f_2 = 5$, $\omega_1/\omega_2 = \sqrt{2}$.

In order to illustrate the proposed method, the proposed optimization formulation in Eq. (15) is used firstly to find the worst resonant response. The objective function in Eq. (15) for the proposed optimization formulation is changed as the maximization of the norm of \mathbf{U} . The unknown variables that have to be determined are the unknown Fourier coefficients \mathbf{U} and the worst resonant response frequency ω_1 .

Based on the reduced space SQP algorithm described in Sect. 2.4, optimization is then performed to search the worst resonant quasi-periodic solution and the parameters of the optimization algorithm are adopted as follows: The tolerances for the objective and constraint functions are both set to 10^{-6} , while the maximum number of generations allowed for the reduced space SQP algorithm is 600. A frequency range of interest from 0.1 to 8 (rad/s) for ω_1 is considered. The maximum number of harmonics is taken as $N_H = 5$ for the Fourier series approximation.

The algorithm stops when convergence is achieved. The convergence of the solution is examined by calculating the residual of $\|g(\mathbf{x})\|_1$ and convergence results of the proposed method regarding the objective and constraint functions are provided in Fig. 4. It can be seen from Fig. 4 that the proposed optimization algorithm required 52 iterations to converge and the residual of $\|g(\mathbf{x})\|_1$ shows an oscillatory behavior.

The optimization results are reported in Fig. 5. It is observed in Figs. 4 and 5 that the maximum resonance peak found by the proposed method is 7.7073 at the nonlinear resonance frequency 4.5349(rad/s). Numer-

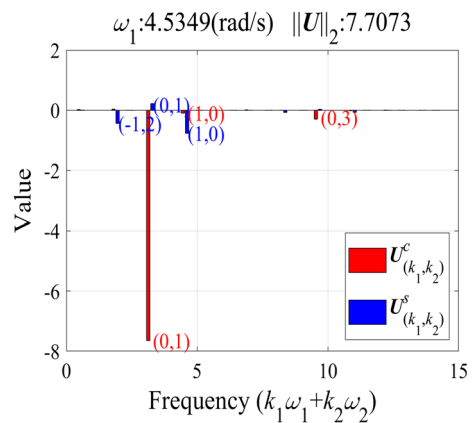


Fig. 5 The optimization results obtained by the proposed method

ical results in Fig. 5 indicate that the most significant contribution in the system response is from the harmonic component $(0,1)$. The harmonic components $(1,0)$ as well as other higher-order harmonic components such as $(-1, 2)$ $(0,3)$ are also excited.

The sensitivity results for the worst-case resonant quasi-periodic solution are reported in Fig. 6. As shown in Fig. 6, the most significant values appear on the diagonal elements of the sensitivity matrix $\frac{\partial g(\mathbf{x})}{\partial \mathbf{U}}$. The sensitivity values are estimated between -1500 and 0. The minimum value is around -1500. For the purpose of validation, sensitivity analysis is performed by using the finite difference method. The sensitivity comparison between the two methods is given in Fig. 7. It is noteworthy that the sensitivity values for $\frac{\partial g(\mathbf{x})}{\partial \mathbf{U}}$ and $\frac{\partial g(\mathbf{x})}{\partial \omega_1}$ obtained by the proposed method are in nearly perfect agreement with the finite difference results although there is small difference between the two methods. The maximum relative difference in Fig. 7

Fig. 6 The sensitivity results obtained by the proposed method

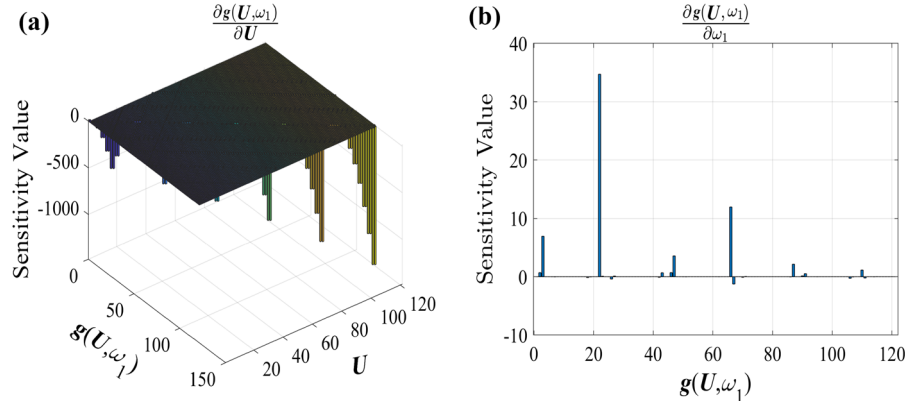
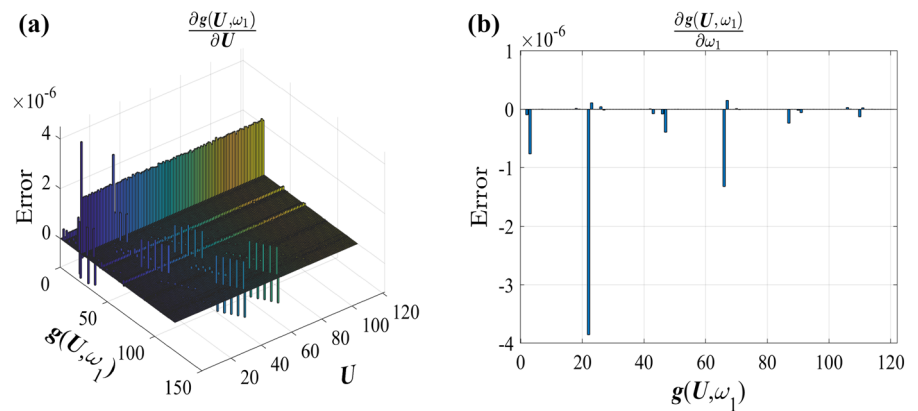


Fig. 7 The comparison of sensitivity results between the proposed method and the finite difference method



is less than 4×10^{-6} . Such agreement provides a qualitative validation of the sensitivity analysis method presented in this article. Therefore, the sensitivity analysis method is validated by comparison with the finite difference method and the quasi-solution prediction based on the proposed method is reliable.

The comparison of sensitivity results between the proposed method and the finite difference method for $\frac{\partial \lambda_1^s}{\partial U_{(k_1, k_2)}^c}$ and $\frac{\partial \lambda_1^s}{\partial U_{(k_1, k_2)}^s}$ is available in Fig. 8 where notations “RSQPHBM” and “finite difference method” represent the solutions obtained by the proposed method and the finite difference method, respectively. Figure 8 shows that the real parts for $\frac{\partial \lambda_1^s}{\partial U_{(k_1, k_2)}^c}$ and $\frac{\partial \lambda_1^s}{\partial U_{(k_1, k_2)}^s}$ are equal to zero. The differences for the sensitivity results between the presented method and finite difference method are negligible. For the imaginary parts, full coincidence of the sensitivity results is observed. It is evident that there is virtually no difference between the two approaches. The sensitivity values of $\frac{\partial \lambda_1^s}{\partial U_{(k_1, k_2)}^c}$ show high magnitude at the harmonic components $(0, 1)$, $(0, 3)$

and $(0, 5)$ while $\frac{\partial \lambda_1^s}{\partial U_{(k_1, k_2)}^s}$ exhibits larger magnitude at the harmonic components $(-1, 2)$, $(-1, 4)$, $(0, 3)$, $(1, 2)$ and $(-1, 6)$. Both the real and imaginary parts of sensitivity results yielded by the proposed method show good agreement with the results calculated by using the finite difference method, which means that the sensitivity results of the proposed method are accurate.

The time history and portrait corresponding to the quasi-periodic solution in Fig. 5 are calculated via numerical integration to validate the proposed method. By means of fourth-order Runge–Kutta method, numerical integration results can be obtained. The time history and the phase space trajectory projection corresponding to the quasi-periodic solution in Fig. 5 are depicted in Fig. 9. In Fig. 9, the time integration method chooses initial condition to be the corresponding optimization solution in Fig. 5. It may be noted from Fig. 9 that the Duffing oscillator has irregular oscillatory behavior. The phase orbit clearly indicates that the system is acted with quasi-periodic motion. Furthermore, the results of the pro-

Fig. 8 Computational error for sensitivity results between the two methods

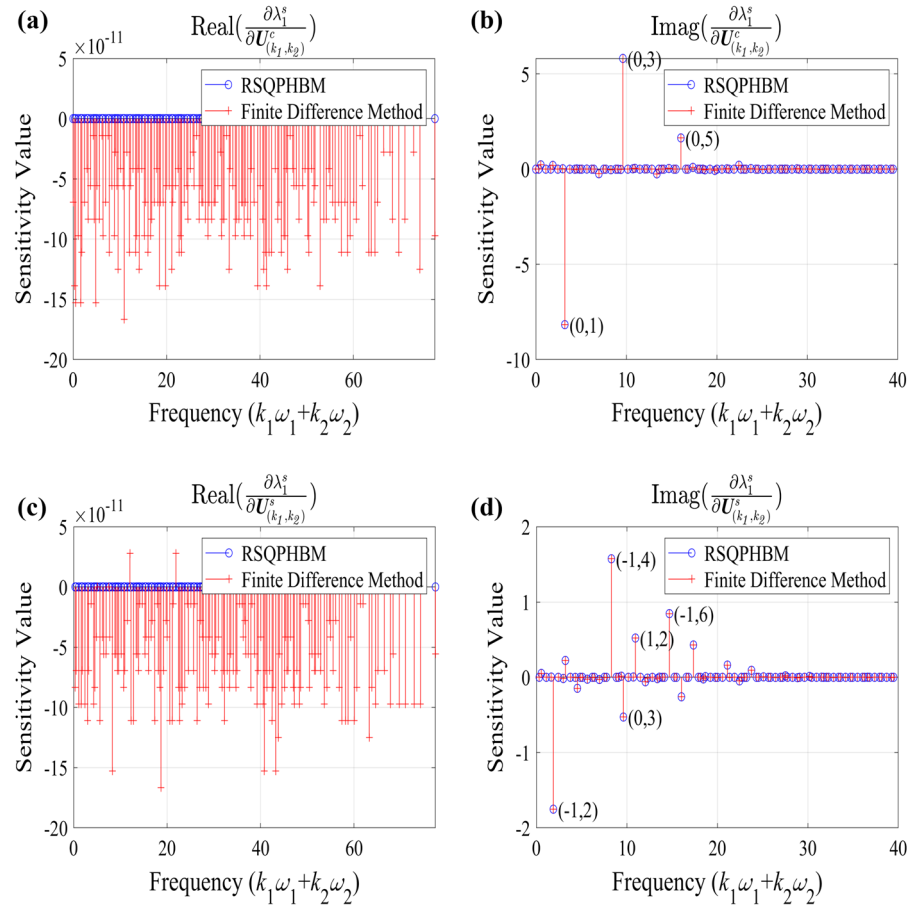
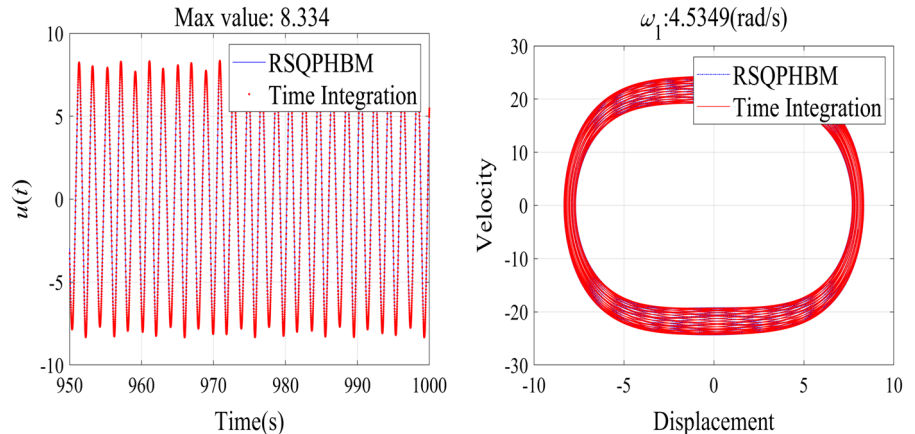


Fig. 9 Time history and phase plane portrait of the peak solution in Fig. 5



posed method match the exact solution of numerical integration method very well. The comparison between the two methods verifies the accuracy of the presented method.

Based on the validations in Figs. 6, 7, 8 and 9, the proposed continuation and stability analysis scheme

can be applied to investigate the dynamic characteristics of quasi-periodic responses. The frequency amplitude response curve obtained by the proposed continuation method is plotted in Fig. 10. For most points in the continuation curve, convergence of the proposed method is observed within several iterations. Figure 10

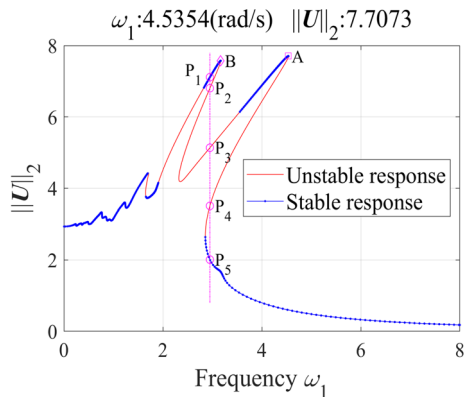


Fig. 10 Frequency response curve of the Duffing oscillator with multi-harmonic forcing

shows that with a hardening spring ($\gamma > 0$) the response curve tends to bend to the right. Unlike the nonlinear frequency response curve with one excitation frequency, two peaks are excited and some regions are multi-values. In addition, it can be noted that the resonance response level has its maximum value 7.7073 at the resonance frequency 4.5354 (rad/s). The worst resonance response results in Fig. 10 are consistent with the optimization results in Fig. 5. Moreover, it is observed that the frequency response curve obtained by the proposed continuation method is nearly identical to Fig. 6 of Ref. [46], and the quasi-periodic solutions have been satisfactorily tracked with the continuation method described in Sect. 2. Therefore, the proposed continuation method has been verified by comparison with the published reference results of Ref. [46].

The results of the proposed stability analysis method are also shown in Fig. 10 where these quasi-periodic solutions are unstable for the red regions and stable for the blue regions. The stability results are interpreted with an allowance of $\varepsilon = 10^{-3}$, with the stability factor $\lambda_1^s > \varepsilon$ implying instability. As illustrated in Fig. 10, the stabilities of quasi-periodic solutions change with the excitation frequency ω_1 . It should be noted that the frequency response curve exhibits unstable behavior in some regions within the frequency range of interest and there are four regions of instability. Particularly, the Duffing system demonstrates unstable quasi-periodic solutions between the two resonant peaks. Compared with the counterparts reported in Ref. [46], the stability behaviors in Fig. 10 are similar to Fig. 9 of Ref. [46] and a concordance between the stability results of Fig. 10 and the corresponding diagram in Fig. 9 of Ref.

[46] can be observed. The proposed stability analysis method qualitatively captures the stability behaviors of quasi-periodic solutions. Regions of stable and unstable quasi-periodic responses appear to be correctly predicted.

The proposed method has the ability for evaluating the stability factors and the accuracy of the stability factor is expected to depend on the selected harmonic number. The number of selected harmonic essentially influences the obtained stability results, i.e., if the quasi-periodic solution is modeled only by a few harmonic, the stability results may be incorrect. Definitely, a higher harmonic would increase the accuracy of the stability judgment, predicting more accurate results. However, it consumes much calculation resources. Therefore, a convergence study is needed to decide an appropriate harmonic number.

The stability factors of quasi-periodic solutions in terms of the excitation frequency are analyzed and the effect of the retained harmonic number N_H on the accuracy of the stability factors is studied in the following. A comparison of the predicted stability factors with different retained harmonic number is depicted in Fig. 11 where the stability behaviors of quasi-periodic solution in Fig. 10 are plotted with $N_H = 5$. Figure 11 shows that the stability curves calculated with difference harmonic number are closer to each other although the differences for some regions are visible, which shows that $N_H = 5$ is precise enough to trace the stabilities of quasi-periodic solutions.

To further assess the performance of the proposed method in terms of the stability characteristics, the stability results for several quasi-periodic solutions at a given frequency are investigated in detail. In Fig. 10, five quasi-periodic solutions coexist at the excitation frequency $\omega_1 = 2.95$ (rad/s) and these cases are examined. Table 1 which also shows the norm of $\|U\|$ and the maximum vibration amplitude u_{\max} summarizes the stability results that are evaluated at these quasi-periodic solutions. In Table 1, λ_j^s represents the Floquet multipliers obtained by using the proposed stability analysis method, and the stability factors with $N_H = 10$ are also listed for the purpose of comparison.

By inspection of the stability factors with $N_H = 5$ and $N_H = 10$ in Table 1, it is worth noting that the proposed method with different N_H yields similar stability results for solutions A, B, P1, P2, P4 and P5. Discrepancy for the stability factors associated with solution P3 is observed but remains very small. The comparison of

Fig. 11 The effect of selected harmonic number on the convergence of the proposed stability analysis method

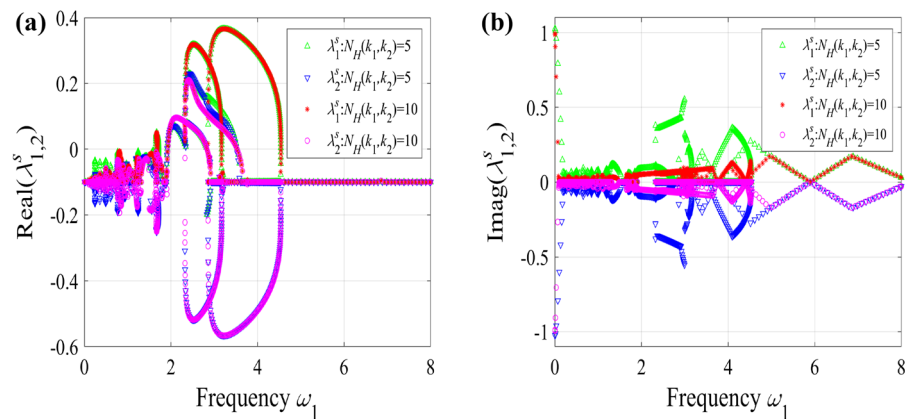


Table 1 Summaries of the stability analysis results

	$N_H = 5$			$N_H = 10$		
	λ_j^s	$\ U\ _2$	u_{\max}	λ_j^s	$\ U\ _2$	u_{\max}
A	$-0.1000 - 0.0541i$	7.7073	$8.334 (\omega_1: 4.5354)$	$-0.1000 - 0.0540i$	7.7072	$8.3308 (\omega_1: 4.5349)$
	$-0.1000 + 0.0541i$			$-0.1000 + 0.0540i$		
B	$-0.1000 - 0.0534i$	7.5756	$8.5855 (\omega_1 : 3.167)$	$-0.1000 - 0.0533i$	7.5747	$8.5955 (\omega_1 : 3.1668)$
	$-0.1000 + 0.0534i$			$-0.1000 + 0.0533i$		
P1	$-0.1000 - 0.1191i$	7.1131	8.2692	$-0.1000 - 0.0081i$	7.1124	8.2859
	$-0.1000 + 0.1191i$			$-0.1000 + 0.0081i$		
P2	$0.2421 + 0.0000i$	6.8045	7.8376	$0.2420 + 0.0000i$	6.8043	7.847
	$-0.4421 + 0.0000i$			$-0.4420 + 0.0000i$		
P3	$0.0880 - 0.4323i$	5.1361	6.4	$0.0730 - 0.2951i$	5.1308	6.3809
	$0.0880 + 0.4323i$			$0.0730 + 0.2951i$		
P4	$0.3201 + 0.0000i$	3.5080	3.9305	$0.3201 + 0.0000i$	3.5077	3.9292
	$-0.5201 + 0.0000i$			$-0.5201 + 0.0000i$		
P5	$-0.1000 - 0.0529i$	2.0098	2.3336	$-0.1000 - 0.0541i$	2.0096	2.3359
	$-0.1000 + 0.0529i$			$-0.1000 + 0.0541i$		

the stability factors with different harmonic number is extremely good and the proposed method predicts the stability factor with good accuracy. Furthermore, the quasi-solutions A, B, P1, and P5 are identified to be stable since the real parts of these stability factors are -0.01 , which are less than zero. These quasi-periodic solutions P2, P3 and P4 are considered unstable as the real parts of these stability factors are positive.

Focusing on the validation of the stability behaviors of quasi-periodic solutions predicted by the proposed stability analysis approach, the quasi-periodic responses for these optimal solutions in Table 1 are compared with the time-domain integration results. Starting from the initial conditions provided by the

proposed method, time-domain integration of Eq. (41) with fixed time step size 0.001 is performed by using the fourth-order Runge–Kutta integration scheme. The computational results are shown in Figs. 12, 13, 14 and 15 where notation “RSQPHBM” refers to the solutions of the proposed method and notation “Time Integration” represents the numerical integration results.

As shown in Figs. 12, 13, 14, 15, 16 and 17, many loops are seen in the phase plane portraits which are banded attractors. The results for quasi-periodic solutions B, P1, and P5 from the proposed method and from the time-domain integration method are difficult to distinguish when they are plotted on the same graph, demonstrating the stability behaviors of these quasi-

Fig. 12 Time histories and its corresponding phase portraits for quasi-periodic solution B

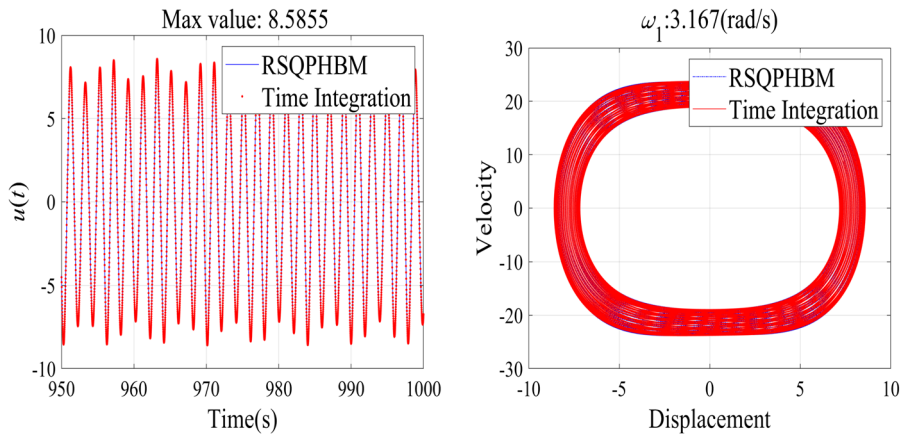


Fig. 13 Time histories and its corresponding phase portraits for quasi-periodic solution P1

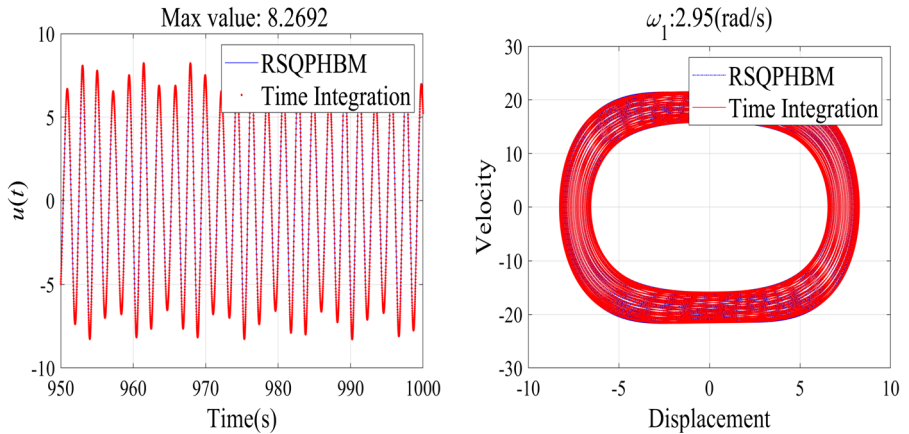
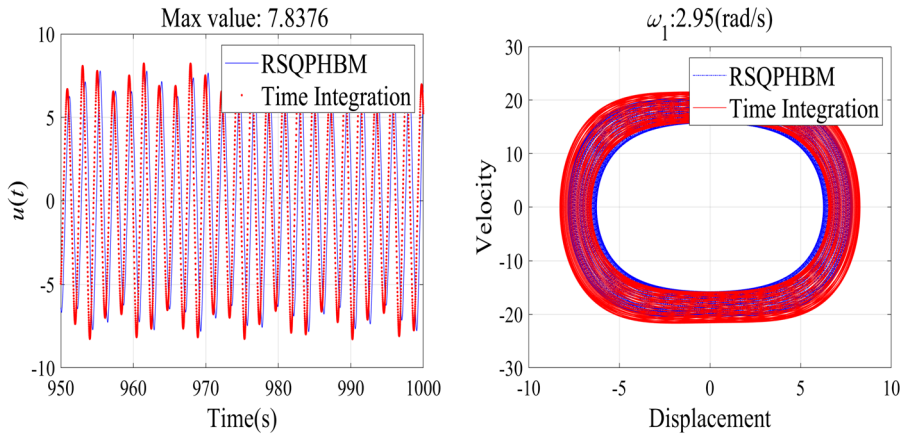


Fig. 14 Time histories and its corresponding phase portraits for quasi-periodic solution P2



periodic solutions. However, quasi-periodic solutions P2, P3, and P4 cannot tracked by the time integration method and these solutions are unstable. Compared with the numerical integration results in Figs. 12, 13, 14, 15, 16 and 17, Table 1 shows that the proposed method gives good estimation of the stability factor and

the stability information is accurately captured. Overall, the proposed stability analysis method in Sect. 3 is verified by comparing with the time-domain integration method.

To explore the sensitivities of the stability factors, the key parameters affecting the stability characteristics

Fig. 15 Time histories and its corresponding phase portraits for quasi-periodic solution P3

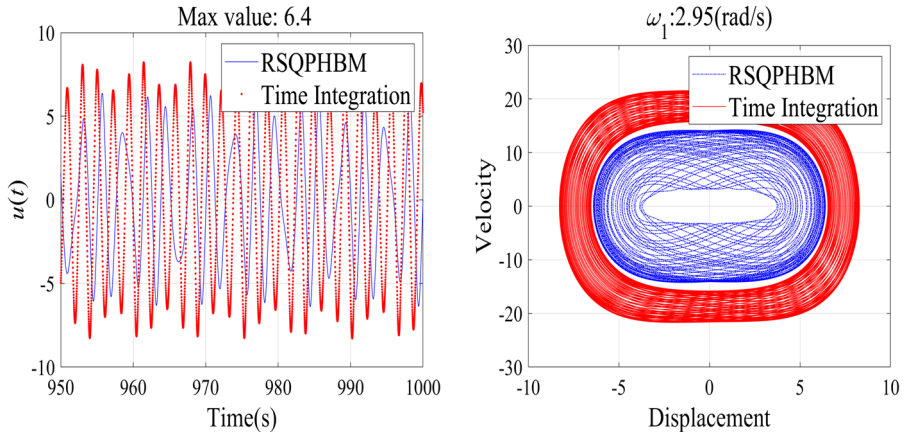


Fig. 16 Time histories and its corresponding phase portraits for quasi-periodic solution P4

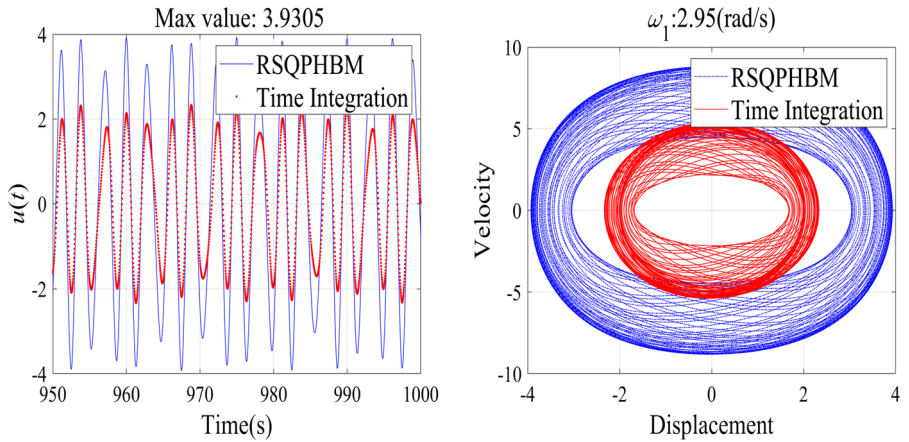
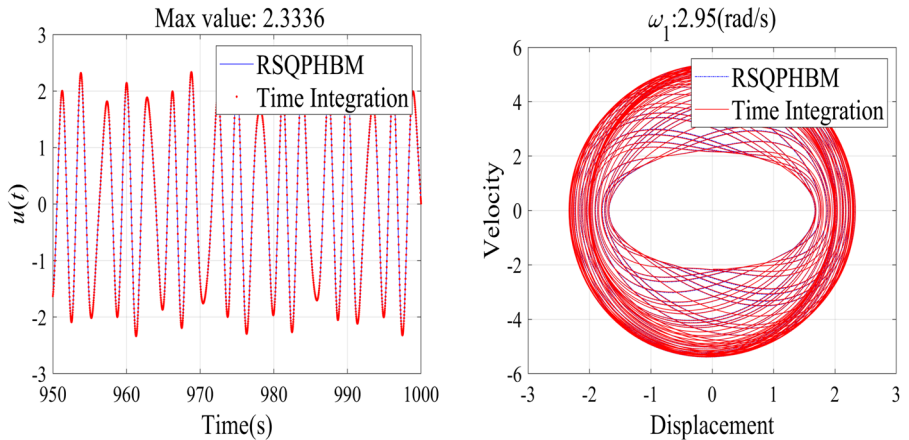


Fig. 17 Time histories and its corresponding phase portraits for quasi-periodic solution P5



are analyzed whereby the influential parameter such as the excitation frequency is varied within its practical range and other input parameters are maintained constant. The real and imaginary parts of the sensitivities $\frac{\partial \lambda_1^s}{\partial \omega_1}$ and $\frac{\partial \lambda_2^s}{\partial \omega_1}$ as a function of the excitation frequency ω_1 are plotted in Fig. 18. As shown in Fig. 18, the

sensitivity values exhibit fluctuations at lower frequencies and the sensitivities at lower frequencies are relatively much higher than that at higher frequencies. In addition, it should be noted that for frequencies where the bifurcations occur there is an evident sharp change of the sensitivity coefficients. The bifurcation points

Fig. 18 Sensitivity results of the stability factor with respect to the excitation frequency

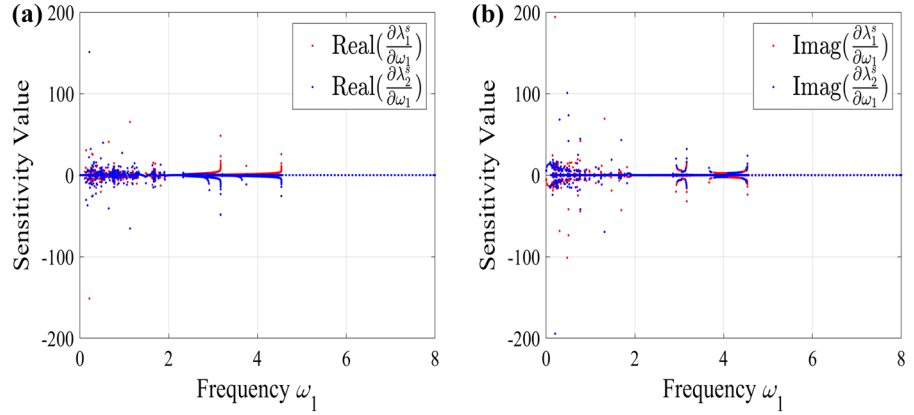
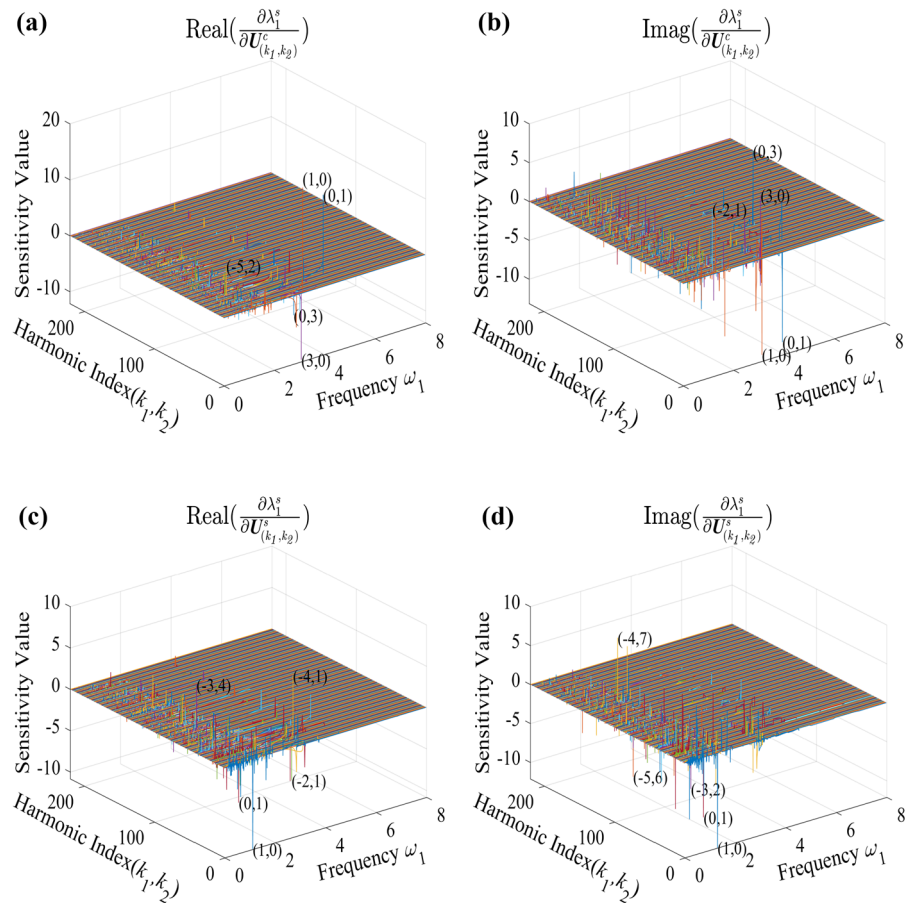


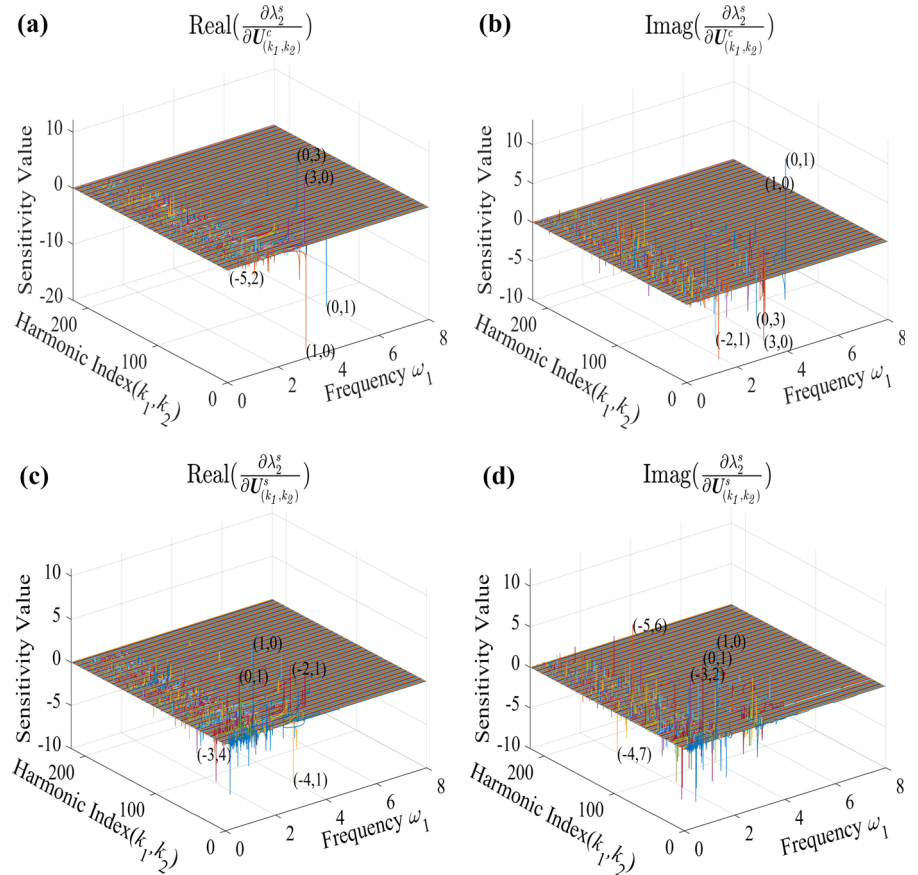
Fig. 19 The sensitivity results as a function of ω_1 for different harmonic index (k_1, k_2)



have very large sensitivity values. The sensitivity of the bifurcation points implies that the Jacobian matrix in Eq. (16) may close to singularity. Therefore, it can be concluded that quasi-periodic solution related to bifurcation point may sensitivity to the variation of structural parameters.

The sensitivities of the stability factors with respect to the Fourier coefficients is depicted in Fig. 19 by plotting the real and imaginary parts of $\frac{\partial \lambda_1^s}{\partial U_{(k_1, k_2)}^{c(s)}}$ against the excitation frequency. As illustrated in Fig. 19, minor peaks with significant values are observed in the sensitivity results. The component of the first excitation

Fig. 20 The sensitivity curves for different harmonic index (k_1, k_2)



frequency ω_1 , the component of the second excitation frequency ω_2 , as well as their coupled components can all be found in the sensitivity curves. It is apparent that the harmonic combinations of $(1,0)$, $(0,1)$ which are dominant in all sensitivity curves exhibit larger sensitivities. For $\frac{\partial \lambda_1^s}{\partial U_{(k_1, k_2)}^c}$, higher harmonic components with prominent harmonic combinations $(3,0)$, $(0,3)$ can be seen in Fig. 19a, b, which highlights the effect of higher-order harmonic components on the sensitivity factor of $\frac{\partial \lambda_1^s}{\partial U_{(k_1, k_2)}^c}$. For the real parts of $\frac{\partial \lambda_j^s}{\partial U_{(k_1, k_2)}^s}$, the sensitivities of harmonic combinations $(-3, 4)$, $(-4, 1)$ and $(-2, 1)$ are more significantly than that of other combinations. Similarly, higher sensitivity values related to higher-order harmonic combinations $(-4, 7)$, $(-5, 6)$ and $(-3, 2)$ are shown in Fig. 19d for the imaginary parts of $\frac{\partial \lambda_j^s}{\partial U_{(k_1, k_2)}^s}$.

In contrast, the computed real and imaginary parts for $\frac{\partial \lambda_2^s}{\partial U_{(k_1, k_2)}^{(G)}}$ are shown in Fig. 20. As shown in Fig. 20a, b

the sensitivity curves contain many smaller peaks particularly at the smaller frequency range. Only some harmonic combination components have significant sensitivity amplitudes. In addition, it is indicated in Fig. 20a, b that the harmonic components $(1,0)(0,1)$ show the highest sensitivity. For $\frac{\partial \lambda_2^s}{\partial U_{(k_1, k_2)}^c}$, the harmonic components $(3,0)(0,3)$ are found to be the significant factor affecting the system stability performance. On the contrary, the stability factor λ_2^s is sensitive to the deviation of high-order harmonic combinations $(-4, 1)$ $(-3, 4)$ $(-2, 1)$ in Fig. 20c which show significant higher sensitivity values. Similar phenomenon is also shown in Fig. 20d.

The reduced space SQP method is combined with multi-dimensional harmonic balance technique to follow the quasi-periodic solutions of Duffing oscillator. The comparison of sensitivity indices calculated from the proposed method and finite difference method verifies the accuracy of the presented method and the aperiodic solutions can be traced as well. Moreover, the sta-

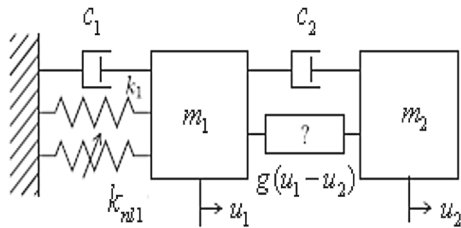


Fig. 21 The profile of the nonlinear tuned vibration absorber coupled to a Duffing oscillator

bility of quasi-periodic solutions predicted by the proposed method is in excellent agreement with the time integration results, and the sensitivity of the stability factor is analyzed. The effectiveness of the proposed method is verified.

4.2 A nonlinear two-degree-of-freedom model

In order to further confirm the feasibility of the proposed method, simulation studies on the quasi-periodic motions for the structural model shown in Fig. 21 are undertaken. The primary system u_1 in Fig. 21 is subjected to the harmonic excitation of $F \cos(\omega_1 t)$. $g(u_1 - u_2) = k_{nl}(u_1 - u_2)^3$ with k_{nl} denoting the nonlinear stiffness coefficient is the nonlinear function of the displacement relative to u_1 and u_2 .

The equations of motion for this two-DOF system can be easily established as

$$\begin{aligned} m_1 \ddot{u}_1 + c_1 \dot{u}_1 + k_1 u_1 + k_{nl} u_1^3 + c_2 (\dot{u}_1 - \dot{u}_2) \\ + k_2 (u_1 - u_2) + g(u_1 - u_2) = F \cos(\omega_1 t) \\ m_2 \ddot{u}_2 + c_2 (\dot{u}_2 - \dot{u}_1) + k_2 (u_2 - u_1) - g(u_1 - u_2) = 0 \end{aligned} \quad (42)$$

where m_i , c_i , and k_i ($i = 1, 2$) are, respectively, the mass, damping, and stiffness coefficients.

The system parameters for the model in Fig. 21 are listed in Table 2, which is borrowed from Refs. [50, 51]. This system exhibits rich dynamic characteristics. The first-order and second-order natural frequencies of the underlying linear system are located at $f_1 = 0.8731$ (rad/s) and $f_2 = 1.0913$ (rad/s), respectively. The frequency range of interest is chosen as (0, 1, 6), and this frequency range covers the first-order and second-order resonances excited by the external forcing. The forcing amplitude is kept constant $F = 0.11$.

In order to provide a reference and validation for the present method, periodic responses related to the

Table 2 Physical parameters for the mechanical system used in the simulations

Parameter	Primary system	NLTVA
Mass (Kg)	$m_1 = 1$	$m_2 = 0.05$
Linear stiff (N/m)	$k_1 = 1$	$k_2 = 0.0454$
Linear damping (Ns/m)	$c_1 = 0.002$	$c_2 = 0.0128$
Nonlinear stiff (N/m ³)	$k_{nl1} = 1$	$k_{nl2} = 0.0042$

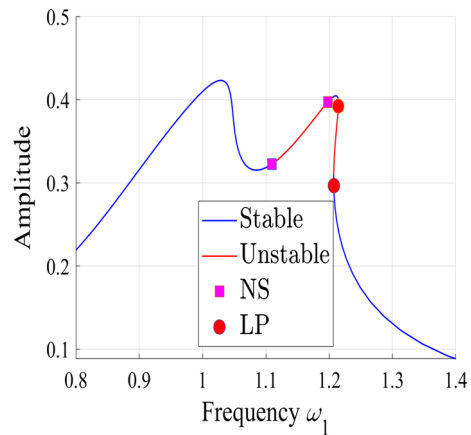
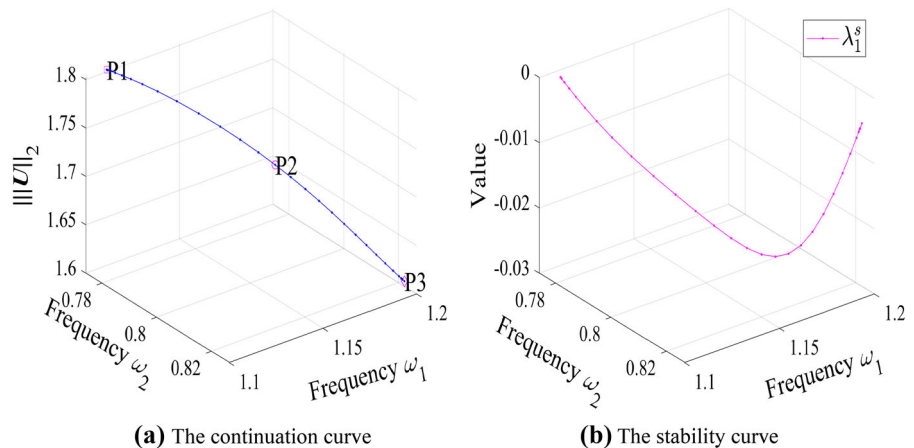


Fig. 22 The frequency response curve obtained by using the continuation method

structure in Table 2 are calculated as a function of the excitation frequency ω_1 . The frequency response curve is constructed from the continuation method and displayed in Fig. 22 for the first Dof u_1 where blue and red lines represent the stable and unstable solutions, respectively. The continuation of the periodic motion is accomplished by the pseudo-arc length continuation method. The stability analysis is carried out by using the Hill method. Notations NS and LP in Fig. 22 stand for Neimark–Sacker bifurcation and limit point bifurcation in structural dynamics.

As illustrated in Fig. 22, two resonance peaks are observed and the first resonance peak is reached at $\omega_1 = 1.0288$ (rad/s). The resonant frequencies vary but stay close to the first-order and second-order natural frequencies of the underlying linear system. Stability analysis shows that some part of the frequency response curve can be stable. The motions of the system exhibit complex response in region of $1.1 < \omega_1 < 1.2$. The Neimark–Sacker bifurcation appears and the Limit point bifurcation also exists. The appearance of Neimark–Sacker bifurcation indicates the transition

Fig. 23 The frequency response and stability curves for quasi-periodic solutions



from periodic to quasi-periodic motions. The periodic motions between the two Neimark–Sacker bifurcation points are unstable and replaced by quasi-periodic motions.

In the following, continuation tracking based on the proposed methods in Sects. 2 and 3 is performed to follow quasi-periodic solutions in Fig. 22. The maximum order of $N_H = 10$ is selected, which compromises the balance of numerical accuracy and convergence. In order to provide the initial solutions used for the proposed continuation procedure, the objective function of the optimization scheme in Eq. (15) is changed to maximize the norm of Fourier coefficients U at a given frequency of ω_1 . With the obtained initial solutions, the quasi-periodic continuation curves are generated and shown in Fig. 23 where the stabilities of quasi-periodic solutions are also depicted. As illustrated in Fig. 23, a branch of quasi-periodic motion is observed in the frequency interval $\omega_1 \in [1.1, 1.2]$ (rad/s), which lies between the two NS bifurcation points in Fig. 22. Moreover, the continuation curve experiences a monotonous change with the two frequencies. In addition, Fig. 23 show that all the Floquet multipliers are less than or equal to 0, and therefore the aperiodic solutions are stable. Furthermore, the value of the stability factor λ_1^s decreases dramatically with increasing ω_1 and ω_2 while further increasing ω_1 leads to the increasing of λ_1^s .

Figure 24 illustrates the frequency spectra for the three solutions P1, P2 and P3 in Fig. 23a. As shown in Fig. 24, the quasi-periodic responses turn out to be mainly affected by the low order harmonic components. The highest contribution to the quasi-periodic solutions comes from the first harmonic component (1,0) and the harmonic combinations (-1, 3) and (-3, 3) are

excited. The values related to the harmonic component (1,0) are larger than that of other harmonic combinations.

The quasi-periodic solutions in Fig. 24 are checked by direct numerical integration of the equations of motion given in Eq. (42). Figure 25 displays the time histories and portraits of u_1 for the three solutions in Fig. 24, in which the initial conditions are provided by the proposed method. As illustrated in Fig. 25, the time waveforms show irregular vibration behaviors and the phase plots are symmetric with respect to the coordinate line. Unlike the periodic solutions, multi-looped orbits are shown in Fig. 25 which indicates that these motions are quasi-periodic. In addition, the trajectories obtained by the two methods are coincided with each other, and it is difficult to distinguish the difference between the two methods. The comparison between the two methods verifies the accuracy of the presented method. Furthermore, time-domain analysis results show a good consistency with the solutions obtained by the proposed method, which validates the stability analysis results in Fig. 23b.

The sensitivities of the stability factor with respect to the Fourier coefficients for different harmonic combinations are processed by the proposed method. The analytical sensitivities of $\frac{\partial \lambda_1^s}{\partial U_{kj}^{c(s)}}$ for quasi-periodic solution P2 are compared with the finite difference sensitivities in Fig. 26 where the imaginary parts of the sensitivities which approach to zero are not plotted. As can be seen in Fig. 26, it is evident that the sensitivity results obtained with the proposed method match the finite difference sensitivities very well, which verifies the presented sensitivity analysis method. Besides,

Fig. 24 The harmonic contents for the three quasi-periodic solutions in Fig. 23a

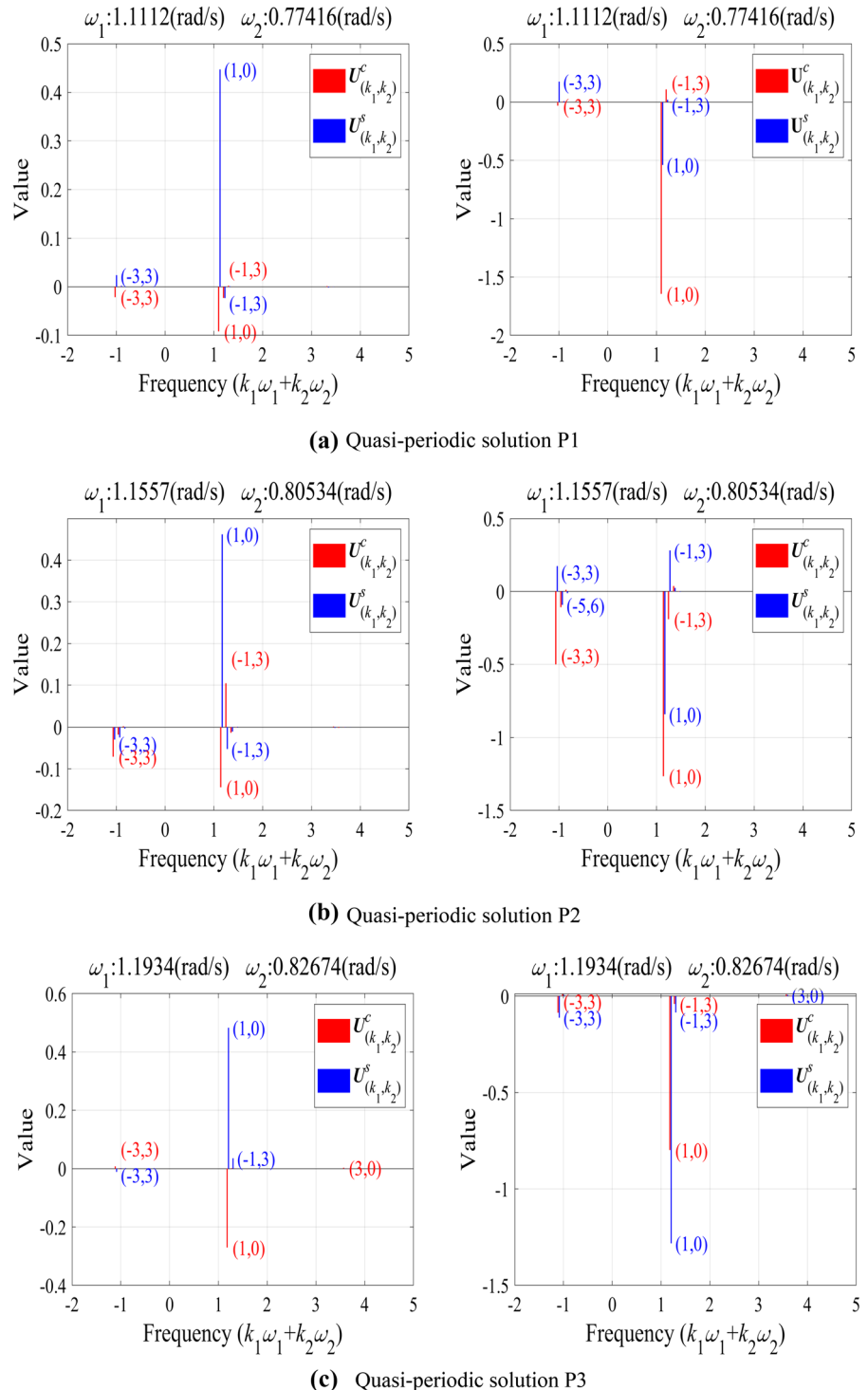


Fig. 25 Time histories and its corresponding phase portraits for the quasi-periodic solutions in Fig. 24

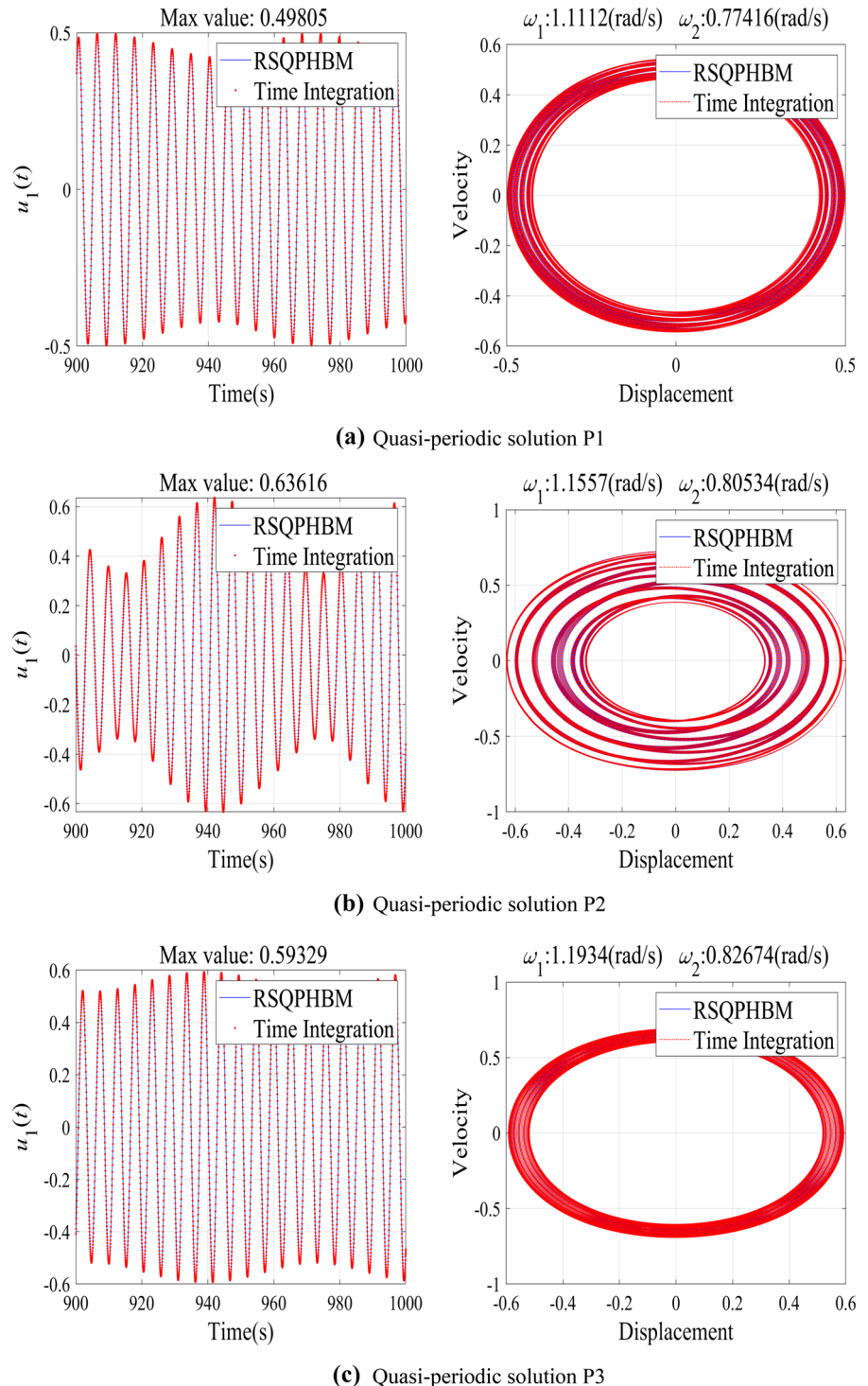


Fig. 26 The sensitivity comparison between the proposed method with finite difference method for quasi-periodic solution P2

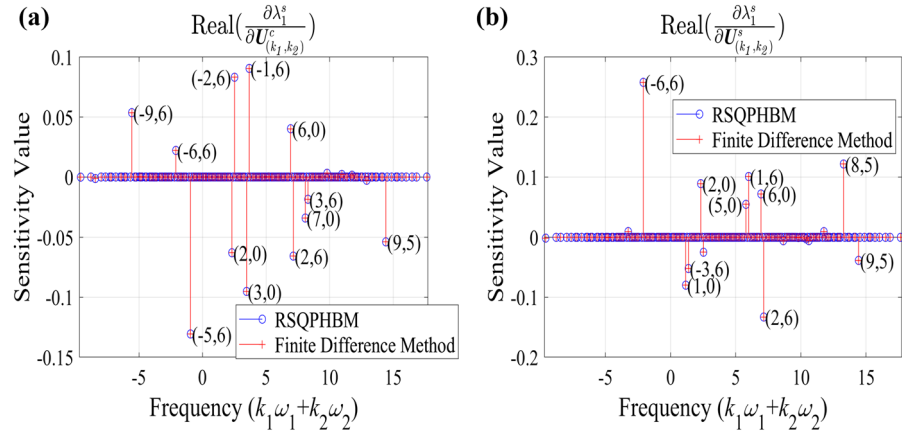


Fig. 27 The sensitivity curves for $\frac{\partial \lambda_1^s}{\partial \omega_1}$ and $\frac{\partial \lambda_1^s}{\partial \omega_2}$

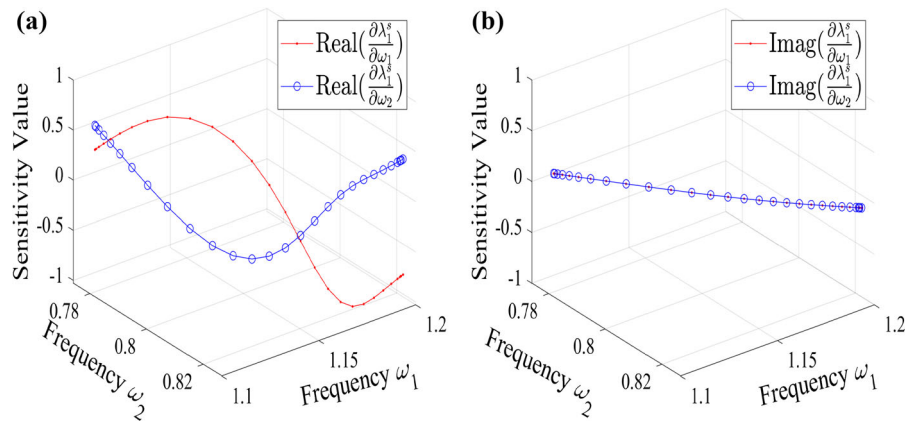


Fig. 26 shows that the sensitivities are more complicated and contain many higher-order harmonic combinations. For the real part of $\frac{\partial \lambda_1^s}{\partial U_{k,j}^c}$ the harmonic component $(-5, 6)$ shows the highest sensitivity value, while the sensitivity value of $\frac{\partial \lambda_1^s}{\partial U_{k,j}^s}$ associated with the harmonic combination $(-6, 6)$ is higher than that of other harmonic combinations. It is noted that the higher-order combinations perform the dominant effect on the sensitivity properties of the stability factor.

Figure 27 plots the real and imaginary parts of the sensitivity coefficients for $\frac{\partial \lambda_1^s}{\partial \omega_1}$ and $\frac{\partial \lambda_1^s}{\partial \omega_2}$ as functions of ω_1 and ω_2 . It can be observed in Fig. 27 that the sensitivity amplitude of $\text{Real}(\frac{\partial \lambda_1^s}{\partial \omega_1})$ firstly increases with the two frequencies and reaches the peak, and then decreases sharply. On the contrary, the sensitivity magnitude of $\text{Real}(\frac{\partial \lambda_1^s}{\partial \omega_2})$ decreases to a minimum value and then begins to increase. However, the imaginary parts of the stability sensitivity

coefficients are almost equal to zero, which is not so complicated as the real parts of sensitivity coefficients.

Sensitivities of the stability criterion with respect to the Fourier coefficients are displayed in Fig. 28 for u_1 . As illustrated in Fig. 28, the computed gradients appear to be a smooth function of the excitation frequency ω_1 . The real parts of the sensitivities are small for most harmonic combinations but for some combinations higher sensitivity values can be seen. The sensitivities corresponding to harmonic combinations $(1,0)$, $(-5, 6)$, $(1,3)$ and $(-1, 6)$ have higher values. However, the imaginary parts of sensitivities are relatively very small, which approach to zero.

The sensitivity computational results for the second Dof u_2 are visualized in Fig. 29. Similar to the previous test case, remarkable sensitivity amplitudes can be perceived in real parts, and the imaginary parts of the sensitivity coefficients are not sensitive to the variation of harmonic coefficients. As shown in

Fig. 28 Sensitivity results of the stability factor for u_1

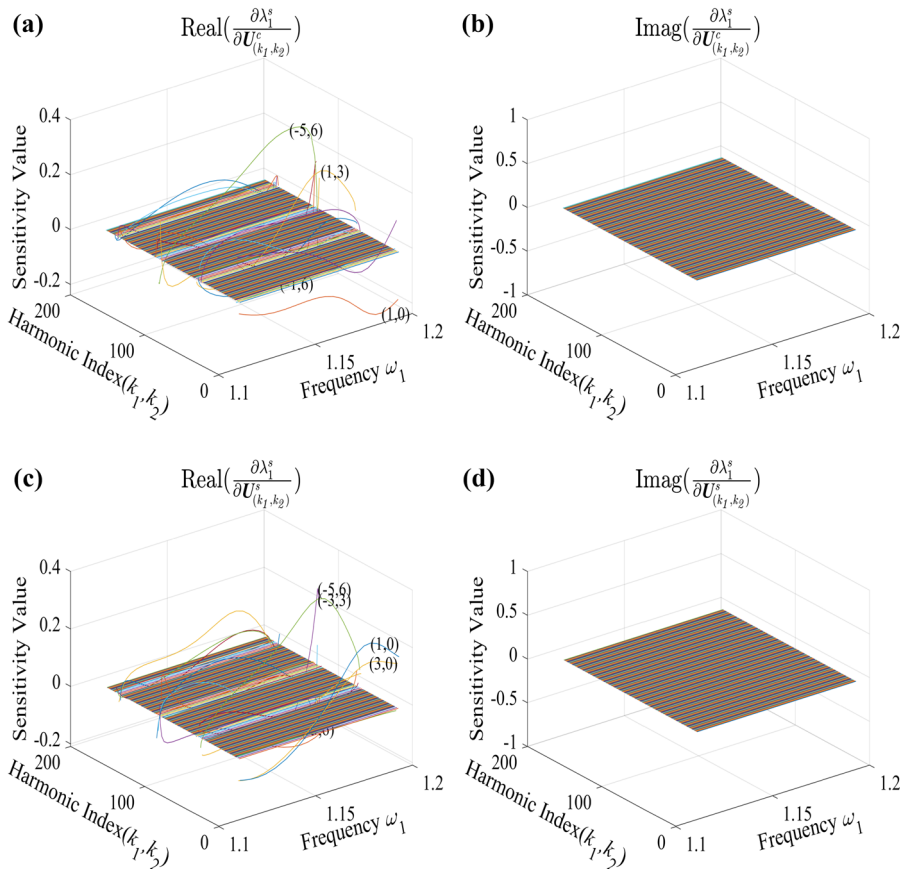


Fig. 29, the first five influential harmonic combinations $(1,0), (-5,6), (1,3), (-1,6)$ have higher values of the sensitivity coefficients. Other harmonic combinations have almost negligible effects on the stability sensitivity.

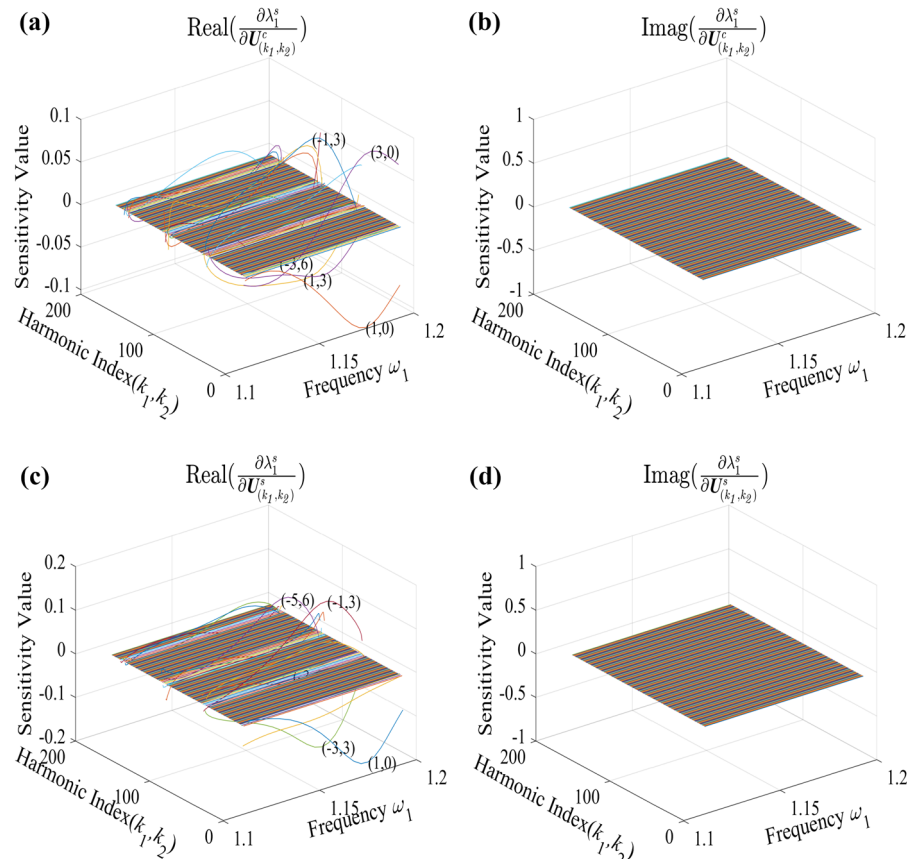
In this paper, a novel strategy to merge the reduced space SQP method and the multi-dimensional harmonic balance method is proposed to follow quasi-periodic solutions of nonlinear systems. The key features of the proposed continuation scheme are the use of the reduced space SQP method within the predictor–corrector continuation framework. The predictive results of the proposed stability analysis method are compared with the counterparts obtained by the time integration method. It is evident that the stability behavior predicted by the presented approach match well with that of the numerical integration method and the feasibility of the proposed methods is proved. Therefore, the proposed methods are utilized.

5 Conclusions

In the present study, the numerical continuation method and stability analysis technique for quasi-periodic solutions of nonlinear systems are proposed. The quasi-periodic solution is tracked by using the reduced space SQP method in conjunction with the multi-dimensional harmonic balance method. The correction step for the continuation problem is tackled as the nonlinear constrained optimization problem with the harmonic balance equations as the nonlinear equality constraints and the reduced space SQP method is adopted to obtain the quasi-periodic solution of nonlinear systems. In order to improve the computational efficiency of the reduced space SQP algorithm, the analytical gradients about the harmonic balance algebraic system are derived.

A novel stability analysis method based on the Floquet theory is developed to predict the stability of quasi-periodic solutions. By employing the harmonic balance formulation with the perturbation

Fig. 29 Sensitivity results of the stability factor for u_2



method, the eigenvalue problem for assessing the stability of quasi-periodic solutions is established and system stability can be judged from the real parts of the Floquet multipliers. In addition, the sensitivities of the stability criterion with respect to the influence parameters are analyzed. The implementations of the proposed methods on two numerical examples are reported. Numerical results confirm that the gradient-based method can successfully be used in conjunction with the multi-dimensional harmonic balance method to track the quasi-periodic solutions and the proposed stability analysis method is efficient and accurate in comparison with the time-domain integration approach.

Two aspects of the proposed methods give its novelty: Firstly, the nonlinear constrained optimization method is used to trace the quasi-periodic solutions, as opposed to the Newton–Raphson method, to make the continuation tracking problem of quasi-periodic solutions less requirement and hence more suitable for industrial applications. Secondly, the sta-

bility of the quasi-periodic solutions is investigated by studying the evolution of perturbations to the known quasi-periodic solution and the advantages of the stability analysis technique are its efficiency in the frequency domain for estimating the stability of quasi-periodic motions. By virtue of the previous mentioned merits, future works will be devoted to apply the proposed methods for tracking quasi-periodic solutions of nonlinear systems with multi parameters.

Acknowledgements The research reported here has received funding from the National Science Foundation of China under Grants (No. 11972082), the Beijing Municipal Science and Technology Project (Z181100004118002) and the Beijing Institute of Technology Research Fund Program for Young Scholars which are highly appreciated by the authors.

Compliance with ethical standards

Conflict of interest The authors declare that they have no conflict of interest.

References

1. Awrejcewicz, J., Someya, T.: Periodic, quasi-periodic and chaotic orbits and their bifurcations in a system of coupled oscillators. *J. Sound Vib.* **146**(3), 527–532 (1991)
2. Awrejcewicz, J.: Numerical analysis of the oscillations of human vocal cords. *Nonlinear Dyn.* **2**(1), 35–52 (1991)
3. Awrejcewicz, J.: Three routes to chaos in simple sinusoidally driven oscillators. *ZAMM J. Appl. Math. Mech.* **71**(2), 71–79 (1991)
4. Sharma, A., Sinha, S.C.: Control of nonlinear systems exhibiting chaos to desired periodic or quasi-periodic motions. *Nonlinear Dyn.* **99**, 559–574 (2019)
5. Breunung, T., Haller, G.: When does a periodic response exist in a periodically forced multi-degree-of-freedom mechanical system. *Nonlinear Dyn.* **98**, 1761–1780 (2019)
6. Yuan, T.C., Yang, J., Chen, L.Q.: A harmonic balance approach with alternating frequency/time domain progress for piezoelectric mechanical systems. *Mech. Syst. Signal Process.* **120**, 274–289 (2019)
7. Leung, A.Y.T., Guo, Z.: Residue harmonic balance approach to limit cycles of non-linear jerk equations. *Int. J. Nonlinear Mech.* **46**, 898–906 (2011)
8. Ranjbarzadeh, H., Kakavand, F.: Determination of nonlinear vibration of 2DOF system with an asymmetric piecewise-linear compression spring using incremental harmonic balance method. *Eur. J. Mech. A/Solids* **73**, 161–168 (2019)
9. Jahn, M., Tatzko, S., Panning-von Scheidt, L., et al.: Comparison of different harmonic balance based methodologies for computation of nonlinear modes of non-conservative mechanical systems. *Mech. Syst. Signal Process.* **127**, 159–171 (2019)
10. Wang, X., Zhu, W., Zhao, X.: An incremental harmonic balance method with a general formula of jacobian matrix and a direct construction method in stability analysis of periodic responses of general nonlinear delay differential equations. *J. Appl. Mech.* **86**(6), 061011 (2019)
11. Zhou, S., Song, G., Li, Y., et al.: Dynamic and steady analysis of a 2-DOF vehicle system by modified incremental harmonic balance method. *Nonlinear Dyn.* **98**, 75–94 (2019)
12. Liao, H., Sun, W.: A new method for predicting the maximum vibration amplitude of periodic solution of non-linear system. *Nonlinear Dyn.* **71**(3), 569–582 (2013)
13. Liao, H.: Optimization analysis of Duffing oscillator with fractional derivatives. *Nonlinear Dyn.* **79**(2), 1311–1328 (2015)
14. Liao, H., Wu, W., Fang, D.: The reduced space sequential quadratic programming (SQP) method for calculating the worst resonance response of nonlinear systems. *J. Sound Vib.* **425**, 301–323 (2018)
15. Allgower, E.L., Georg, K.: Numerical Continuation Methods: An Introduction. Springer, Berlin (2012)
16. Sarrouy, E., Sinou, J.-J.: Non-linear periodic and quasi-periodic vibrations in mechanical systems—on the use of the harmonic balance methods. In: Ebrahimi, F. (Ed.), Advances in Vibration Analysis Research, INTECH, Open Access Publisher (2011), Chapter 21
17. Krauskopf, B., Osinga, H.M., Galán-Vioque, J.: Numerical Continuation Methods for Dynamical Systems. Springer, Dordrecht (2007)
18. Liu, F., Zhou, J.: Shooting and arc-length continuation method for periodic solution and bifurcation of nonlinear oscillation of viscoelastic dielectric elastomers. *J. Appl. Mech.* **85**(1), 011005 (2018)
19. Renault, A., Thomas, O., Mahe, H.: Numerical antiresonance continuation of structural systems. *Mech. Syst. Signal Process.* **116**, 963–984 (2019)
20. Cochelin, B., Vergez, C.: A high order purely frequency-based harmonic balance formulation for continuation of periodic solutions. *J. Sound Vib.* **324**, 243–262 (2009)
21. Guillot, L., Cochelin, B., Vergez, C.: A Taylor series-based continuation method for solutions of dynamical systems. *Nonlinear Dyn.* **98**, 2827–2845 (2019)
22. Guillot, L., Vergez, C., Cochelin, B.: Continuation of periodic solutions of various types of delay differential equations using asymptotic numerical method and harmonic balance method. *Nonlinear Dyn.* **97**, 123–134 (2019)
23. Guskov, M., Sinou, J.-J., Thouverez, F.: Multi-dimensional harmonic balance applied to rotor dynamics. *Mech. Res. Commun.* **35**, 537–545 (2008)
24. Awrejcewicz, J., Reinhardt, W.D.: Some comments about quasi-periodic attractors. *J. Sound Vib.* **139**, 347–350 (1990)
25. Awrejcewicz, J., Reinhardt, W.D.: Quasiperiodicity, strange non-chaotic and chaotic attractors in a forced two degrees-of-freedom system. *ZAMP J. Appl. Math. Phys.* **41**(5), 713–727 (1990)
26. Awrejcewicz, J.: Quasi-periodic solutions analytical and numerical investigations. *Comput. Assist. Mech. Eng. Sci.* **2**, 1–17 (1995)
27. Jain, S., Breunung, T., Haller, G.: Fast computation of steady-state response for high-degree-of-freedom nonlinear systems. *Nonlinear Dyn.* **97**, 313–341 (2019)
28. Huang, J.L., Zhou, W.J., Zhu, W.D.: Quasi-periodic motions of high-dimensional nonlinear models of a translating beam with a stationary load subsystem under harmonic boundary excitation. *J. Sound Vib.* **462**, 114870 (2019)
29. Liu, G., Lv, Z.R., Liu, J.K., et al.: Quasi-periodic aeroelastic response analysis of an airfoil with external store by incremental harmonic balance method. *Int. J. Non-Linear Mech.* **100**, 10–19 (2018)
30. Zhou, B., Thouverez, F., Lenoir, D.: A variable-coefficient harmonic balance method for the prediction of quasi-periodic response in nonlinear systems. *Mech. Syst. Signal Process.* **64**(5), 233–244 (2015)
31. Kim, Y.B., Noah, S.T.: Quasi-periodic response and stability analysis for a non-linear Jeffcott rotor. *J. Sound Vib.* **190**(2), 239–253 (1996)
32. Fontanella, F., Grolet, A., Salles, L., et al.: Computation of quasi-periodic localised vibrations in nonlinear cyclic and symmetric structures using harmonic balance methods. *J. Sound Vib.* **438**, 54–65 (2019)
33. Liao, H.: Global resonance optimization analysis of nonlinear mechanical systems: application to the uncertainty quantification problems in rotor dynamics. *Commun. Nonlinear Sci. Numer. Simul.* **19**(9), 3323–3345 (2014)
34. Peletan, L., Baguet, S., Torkhani, M., et al.: Quasi-periodic harmonic balance method for rubbing self-induced vibrations in rotor-stator dynamics. *Nonlinear Dyn.* **78**(4), 2501–2515 (2014)

35. Guillot, L., Vigué, P., Vergez, C., et al.: Continuation of quasi-periodic solutions with two-frequency harmonic balance method. *J. Sound Vib.* **394**, 434–450 (2017)
36. Salles, L., Staples, B., Hoffmann, N., Schwingshackl, C.: Continuation techniques for analysis of whole aeroengine dynamics with imperfect bifurcations and isolated solutions. *Nonlinear Dyn.* **86**, 1897–1911 (2016)
37. Alcorta, R., Baguet, S., Prabel, B., et al.: Period doubling bifurcation analysis and isolated sub-harmonic resonances in an oscillator with asymmetric clearances. *Nonlinear Dyn.* **98**, 2939–3960 (2019)
38. Detroux, T., Renson, L., Masset, L., et al.: The harmonic balance method for bifurcation analysis of large-scale nonlinear mechanical systems. *Comput. Methods Appl. Mech. Eng.* **296**, 18–38 (2015)
39. Awrejcewicz, J.: Numerical investigations of the constant and periodic motions of the human vocal cords including stability and bifurcation phenomena. *Dyn. Stab. Sys.* **5**(1), 11–28 (1990)
40. Awrejcewicz, J.: Bifurcation portrait of the human vocal cord oscillations. *J. Sound Vib.* **136**, 151–156 (1990)
41. Seydel, R.: Practical Bifurcation and Stability Analysis. Springer, Berlin (2009)
42. Lu, K., Jin, Y., Chen, Y., et al.: Stability analysis of reduced rotor pedestal looseness fault model. *Nonlinear Dyn.* **82**(4), 1611–1622 (2015)
43. Von Groll, G., Ewins, D.J.: The harmonic balance method with arc-length continuation in rotor/stator contact problems. *J. Sound Vib.* **241**(2), 223–233 (2001)
44. Villa, C., Sinou, J.J., Thouverez, F.: Stability and vibration analysis of a complex flexible rotor bearing system. *Commun. Nonlinear Sci. Numer. Simul.* **13**(4), 804–821 (2008)
45. Peletan, L., Baguet, S., Torkhani, M., et al.: A comparison of stability computational methods for periodic solution of nonlinear problems with application to rotordynamics. *Nonlinear Dyn.* **72**(3), 671–682 (2013)
46. Guskov, M., Thouverez, F.: Harmonic balance-based approach for quasi-periodic motions and stability analysis. *J. Vib. Acoust.* **134**(3), 031003 (2012)
47. Cameron, T.M., Griffin, J.H.: An alternating frequency/time domain method for calculating the steady-state response of nonlinear dynamic systems. *J. Appl. Mech.* **56**, 149 (1989)
48. Wright, S., Nocedal, J.: Numerical Optimization, 2nd edn. Springer, New York (2006)
49. Biegler, L.T., Nocedal, J., Schmid, C., Ternet, D.: Numerical experience with a reduced Hessian method for large scale constrained optimization. *Comput. Opt. Appl.* **15**(1), 45–67 (2000)
50. Habib, G., Detroux, T., Viguié, R., et al.: Nonlinear generalization of Den Hartog's equal-peak method. *Mech. Syst. Signal Process.* **52**, 17–28 (2015)
51. Detroux, T., Habib, G., Masset, L., et al.: Performance, robustness and sensitivity analysis of the nonlinear tuned vibration absorber. *Mech. Syst. Signal Process.* **60**, 799–809 (2015)

Publisher's Note Springer Nature remains neutral with regard to jurisdictional claims in published maps and institutional affiliations.